REPORT DOCUMENTATION PAGE	Form Approved OMB No. 0704-0188

1. REPORT DATE (DD-MM-YYYY)	2. REPORT TYPE	3. DATES COVERED (From - To)
December 2011	Final Technical Report	16-Mar-08 to 31-Dec-11

4. TITLE AND SUBTITLE

Modeling and Synthesis Methods for Retrofit Design of Submarine Actuation Systems

Energy Storage for Electric Actuators

5a. CONTRACT NUMBER

5b. GRANT NUMBER

N00014-08-1-0424

5c. PROGRAM ELEMENT NUMBER

6. AUTHOR(S)

Jonathan R. LeSage, Raul G. Longoria, and William L. Shutt

5d. PROJECT NUMBER

5e. TASK NUMBER

5f. WORK UNIT NUMBER

7. PERFORMING ORGANIZATION NAME(S) AND ADDRESS(ES)

Center for Electromechanics
The University of Texas at Austin
1 University Station R7000
Austin TX 78712

8. PERFORMING ORGANIZATION REPORT NUMBER

RF 319

9. SPONSORING/MONITORING AGENCY NAME(S) AND ADDRESS(ES)

Office of Naval Research
875 North Randolph Street
Arlington VA 22203-1995

10. SPONSOR/MONITOR'S ACRONYM(S)

ONR BD254

11. SPONSOR/MONITOR'S REPORT NUMBER(S)

12. DISTRIBUTION/AVAILABILITY STATEMENT

DISTRIBUTION STATEMENT A. Approved for public release; distribution is unlimited.

13. SUPPLEMENTARY NOTES

14. ABSTRACT

This report describes methods for retrofitting legacy hydraulic systems, particularly evaluating means for generating and verifying retrofit or new system design requirements. Methods that combine physics-based modeling, simulation, and design techniques are described and applied to a submarine control surface actuator retrofit problem. First, an integrated submarine/actuator subsystem model is developed for simulation-based design requirements generation. Simulations are used to derive power and energy storage requirements for control surface actuation during extreme submarine maneuvers, such as emergency surfacing. This study also investigated synthesis methods based on classical impedance synthesis techniques for realizing feasible actuator system configurations based on performance specifications. Application to disturbance rejection demonstrates resulting designs that are purely passive or fully active electromechanical systems. These methods can supplement designs proposed by domain experts, and enable means for choosing different configurations and for initially sizing system components.

15. SUBJECT TERMS

Submarines, electromagnetic actuators, energy storage, simulation-based design, system sizing

16. SECURITY CLASSIFICATION OF:			17. LIMITATION OF ABSTRACT	18. NUMBER OF PAGES	19a. NAME OF RESPONSIBLE PERSON
a. REPORT	b. ABSTRACT	c. THIS PAGE			Robert Hebner
UU	UU	UU	UU	58	19b. TELEPHONE NUMBER (Include area code) 512-232-1628

Modeling and Synthesis Methods for Retrofit Design of Submarine Actuation Systems

Energy Storage for Electric Actuators
Grant No: N00014-08-1-0424

Submitted by:

Jonathan R. LeSage, Raul G. Longoria, and William L. Shutt

Prepared Under the Direction of
Robert E. Hebner[4]
Electric Ship Research and Development Consortium

Report Submitted to:

Office of Naval Research

Center for Electromechanics
The University of Texas at Austin
1 University Station, R7000
Austin TX 78712

December 15, 2011

Executive Summary This report describes a study motivated by the need to replace legacy hydraulic systems with sustainable, lower-cost, technology insertions. There have recently been reports on demonstrated electrical actuator systems that are able to meet nominal requirements set forth by the U.S. Navy [1], and these systems have or will soon begin to undergo testing[5]. The goal of this study was to take a different perspective on the retrofit problem, working instead on evaluating means for generating and/or verifying retrofit or new system design requirements. The intent was to develop physics-based modeling, simulation, and design techniques that could support the efforts being taken to develop and/or identify appropriate control surface actuator technologies.

Two primary approaches were taken. First, an integrated submarine/actuator subsystem model was developed as a platform for simulation-based design requirements generation. The utility of this method was demonstrated by determining the power and energy storage requirements for a control surface actuation system by simulating known extreme submarine maneuvers, such as emergency surfacing. Example power requirements for an actuator system for a Virginia class submarine were found to be 150 kW in four quadrant operation (with a power limit of 237 kW) during full sweep maneuvering. Additionally, estimates of local energy storage requirements in the event of systematic power failure were found to be 80 kJ for an emergency surfacing.

This study also investigated synthesis methods for realizing possible actuator system configurations based on performance specifications. The intent of this work was to evaluate tools that could support the retrofit process. The specific methods adopted are based on classical impedance synthesis techniques, first used in design of passive and active electrical circuits. In this work, it is demonstrated how these concepts can be extended to provide design candidates for electromechanical systems, as might be needed for control surface actuation. This study demonstrates how actuator system design candidates can be formulated by considering the case of ocean disturbances rejection during control of a nominal trajectory. The application to disturbance rejection shows how these techniques can provide design alternatives that achieve this function either through a purely passive design, which consumes no additional power, or by using a fully active electromechanical system. These methods can provide alternatives to systems proposed by domain experts, and enable means for choosing different configurations and initially sizing system components.

[5]Reported February 2011: http://www.onr.navy.mil/en/Media-Center/Fact-Sheets/Payload-Tube-Electric-Actuator.aspx

1 Introduction

As a current priority, the Navy is looking into methods to reduce life cycle costs for future vessel deployment [1, 2]. One such aspect of cost reduction is the replacement of existing onboard control surface hydraulic actuator designs, which have been in service since World War II, with electromechanical actuators. Control surface actuation for shipboard systems has relied heavily on hydraulic systems, taking advantage of legacy design knowledge. However, these hydraulic systems prove costly to construct and sustain. Initial studies suggest whole life costs (WLC) could be reduced by up to 50% [3] due to conversion from hydraulic to electromechanical systems.

A recent physical retrofitting of a hydraulic actuator on a Type 23 Frigate with an electromechanical system was reported by Stafford and Osborne [4]. Two linear actuators were used to control the aft fixed fin stabilizers on the vessel. This appears to be one of the first instances of an electromechanical retrofit on a naval vessel reported in the open research literature. The results of the study demonstrate not only the feasibility of the retrofitting process but also the viability of electromechanical systems in the naval setting.

Further justification for continued deployment of these systems should show the ease of maintainability of electromechanical systems over hydraulics. Hydraulic systems entail additional piping and ancillary power conversion systems, which add considerably to both construction and maintenance overheads. Hydraulic fluids are drained and the system is flushed in a process that takes upward of 48 hours in addition to any typical servicing which would be standard for any actuation system [4]. Moreover, modern electrical actuators employ intelligence maintenance monitoring with integrated sensors and the ability for prognostics on the fly.

Additionally, retrofitting with electromechanical systems is motivated by electrification of shipboard systems, which promises improvements in actuation systems and resolution of problems associated with hydraulic systems. Not only do hydraulic systems add additional energy conversion paths in the submarine system, additional crew training beyond electrical knowledge is required for maintenance and emergency repairs. The study by Stafford and Osborne [4] found that an electromechanical conversion required only two hours a month for planned maintenance requirements, with other hourly reductions resulting from considerable time savings during dockside maintenance [4]. In modern submarines, actuators serve as a synthesis of functions: motion conversion, power conversion, energy storage and system control as shown in Figure 1. Due to the hostile nature of the ocean, control surface actuators must function in strenuous circumstances and ensure functionality for surfacing in event of power failure. Control surface actuators must also be capable of meeting rigorous torques demands during diverse actuation maneuvers while maintaining high levels of reliability and impact tolerance. Other than situations of overheating and extended over-loading conditions, electrical actuators for control surface replacement attained 98.5 percent availability [4].

Furthermore, electromechanical actuators, which are compact and lightweight, are ideal candidates to replace current hydraulic actuators. Due to the relative simplicity and compactness of electromechanical systems, the retrofitted system should yield a reduction in total

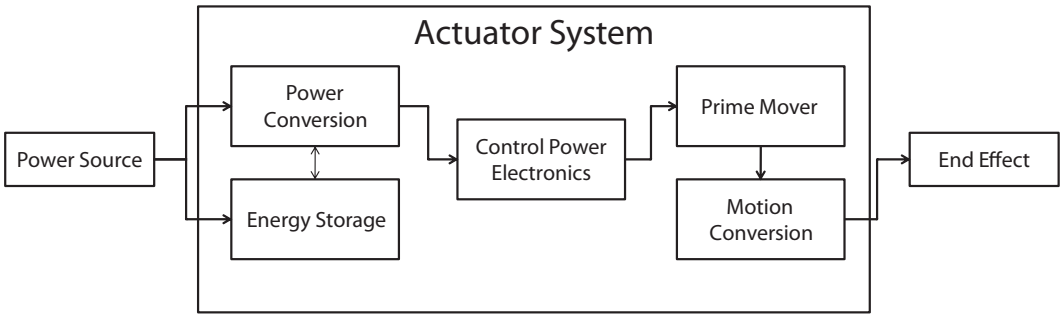

Figure 1: Overall actuation system with vital subdivisions.

actuation system weight. The proposed electromechanical system tested by Stafford and Osborne resulted in a 500 kg weight reduction over the existing hydraulic system [4]. The conversion of electrical voltage generated by the submarine's power plant to hydraulic pressure results in energy loss. Since all energy conversion processes involve a loss in available energy, removal of unnecessary conversion processes results in energy conservation. One potential cause of concern for electromechanical actuation systems is the continuous power consumption present due to actuation position holding. In contrast, hydraulic systems provide continuous position holding with less power consumption. However, the experimental actuation fitting reported in [4] resulted in an electromechanical actuator consuming 11.16 MJ in comparison to the standard hydraulic actuation system, which consumed 23.76 MJ, producing a 53.03% reduction in energy consumption [4].

Since hydraulic actuation in submarines has an extensive history and many system designs and controls have been determined using hydraulics, a technique to determine actuator specifications and component topology is desired. By characterization of the existing hydraulic actuators in both time and frequency domains, electromechanical actuators with identical characteristics can utilize existing control algorithms with indistinguishable responses. Additionally, investigation of the actuation systems must consider submarine system-wide effects on power consumption and motion dynamics. Considerable concentration of mass towards the aft section of the ship results in stability issues for submarine motion.

The Stafford report indicates strong evidence for the favorability of electromechanical system retrofitting. The report presents experimental confirmation of the possibility for a retrofit of existing hydraulic systems with positive benefits. However, many issues and concerns remain unanswered for a finalized retrofit solution such as system component topology, energy storage requirements/placement and power consumption during intense maneuvers. This report addresses each of these problems in turn and explores potential solutions for a final retrofit design in accordance to the specified parameters in Table 1. Since the retrofitting of the control surface actuators suggests system insertion, there is a need for methods to aid formulation of requirements for actuation subsystems that correspond to submarine operational requirements. Modern modeling and simulation tools enable a total systems approach that allows the possibility to propagate overall system response requirements into specified subsystems. However, early or concept design applications requires that physics-based models be developed with minimal design information. Detailed selection and sizing require that requirements be formulated, and it can be helpful to have systematic ways to model and

Table 1: Specified Performance Parameters [1]

Parameter	Specification
Operating Torque Capacity	700,000 ft-lbs (950 kN-m)
Peak Torque Capacity	1,000,000 ft-lbs (1,360 kN-m)
Operational Angular Displacement	± 35 degrees
Rate of Angular Displacement	5 ± 1 deg/s
Position Accuracy	± 0.25 degrees
Energy Storage	1.4 MJ

simulate systems for gaining insight during this process. The following section describes the physics-based model for the submarine model system, which forms a basis for generating key performance requirements from first principles.

2 Submarine Model Development

Physics-based models can be helpful in actuator design assessment since they enable critical power levels to be estimated through simulation studies. This can be especially important in actuation and energy storage sizing, since designers may need to consider power demands imposed by a broad range of external effects [5]. Designers can virtually experiment by imposing changes in the system components and/or environmental conditions as they see fit. In actuator retrofit studies, the dynamics of an existing system (e.g., a legacy hydraulic actuator system) may rely on a power distribution that is radically different from the novel architectures being considered, which could mask new design requirements [4]. For instance, the source impedance of a dc bus system remains intrinsically different to a hydraulic supply line [6]. Physics-based models can help reduce or eliminate any inherent bias or uncertainty associated with this type of retrofit problem. Furthermore, as there may be little to no information available about how an existing system was specified, a physics-based model can provide a more objective basis for making future design decisions, including a way to derive possible duty cycle descriptions for onboard actuator systems. The latter would offer an alternative or basis for comparison to costly full-scale sea trials.

This section summarizes the submarine and control surface actuator models developed for the purpose of this retrofit study. The simulations are based on high fidelity physics-based models meant to provide insight into the interaction between the submarine and actuator dynamics. The simulations can be used to guide electromechanical actuator retrofit requirements. However, these results are only a first step toward a retrofit design, the next step being methods that could support design of a specific actuator system, such as described in Section 4.2.

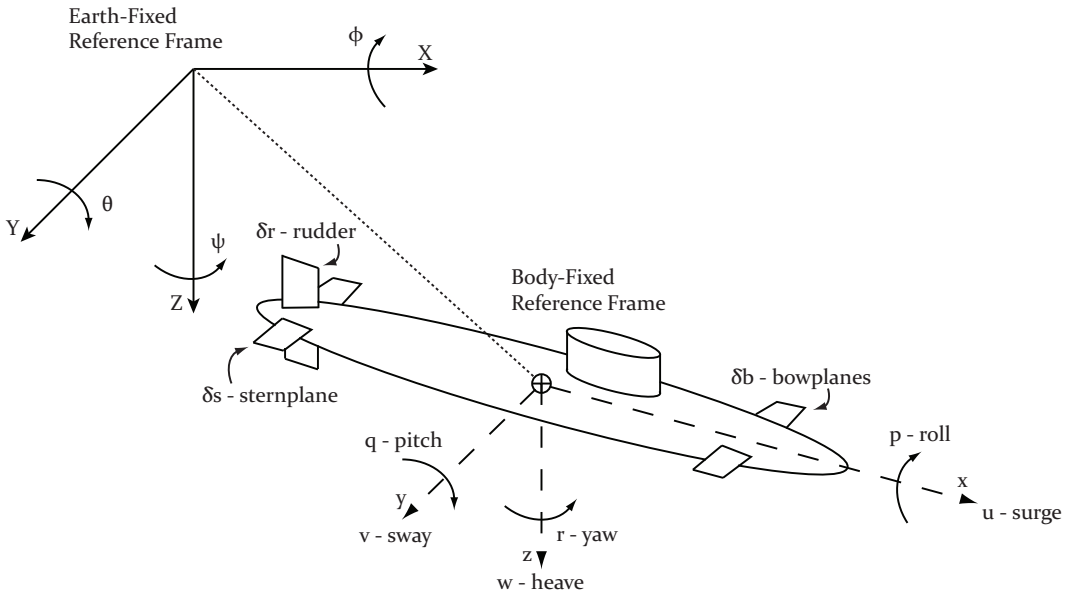

Figure 2: Coordinate frame definitions of submarine vehicular dynamics.

2.1 Six Degree of Freedom Submarine Model

A detailed model of a full six degree of freedom (DOF) submarine system was developed and a simulation implemented using the MATLAB/Simulink environment[6]. For the characterization of energy requirements of actuators, all six degrees of freedom were included to account for all possible internal/external power flow requirements. The body-fixed and global reference frames used in the derivation are illustrated in Figure 2. The high fidelity is necessary as model simplifications will result in gross underestimates of power requirements. As a result, domain-specific knowledge of the system is mandatory for an accurate design assessment. A detailed discussion of the derivation is provided in Appendix A. The force and moment models described in Appendix A.1 form the total forces and moments exerted on the submarine body. A mathematical model in the form of nonlinear ordinary differential equations of motion, with respect to a body-fixed coordinate system, for the submarine takes the form,

$$M\dot{\nu} + C(\nu)\nu + D(\nu)\nu + g(\eta) + g(\nu)u_i = \tau \tag{1}$$

where $M\dot{\nu}$ is the total inertial matrix, $C(\nu)$ is the Coriolis/centripetal matrix, $D(\nu)$ is the total damping matrix, $g(\eta)$ are the buoyancy and weight components, $g(\nu)$ is the control input matrix, and τ is external disturbances. These equations summarize the external forces imposed on the actuation units. The following subsections describe how external forces transfer to the internal actuation systems.

[6]The Mathworks, Inc., 3 Apple Hill Drive, Natick, MA.

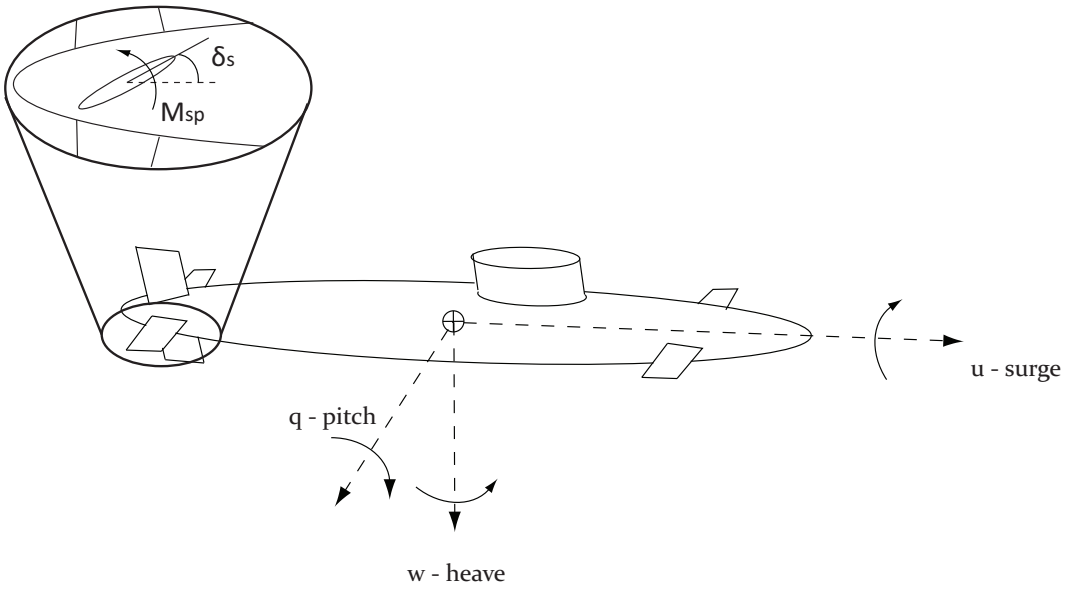

Figure 3: Hydrodynamic moment unit definition.

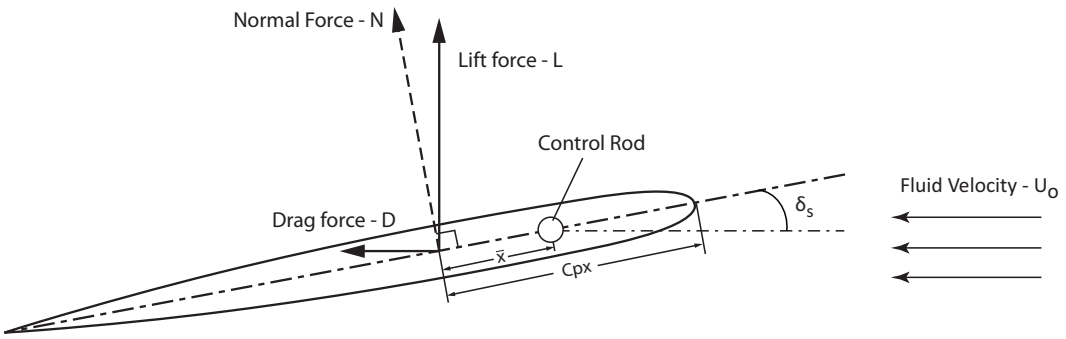

Figure 4: Hydrodynamic lift force and moments imposed on control surface.

2.2 Control Surface Hydrodynamics

Models for representing the control surface hydrodynamic interactions and actuation system were also formulated. The importance of the model equations is twofold. First, the control forces imposed on the submarine motion can be determined, see Figure 3. Second and more importantly, the reaction forces imposed on the actuators due to submarine motion and ocean disturbances can be found. These force transmissions are key for the identification of actuator power requirements [5]. Much akin to an airfoil, the control surface experiences both hydrodynamic lift and drag, see Figure 4. Since we operate under the assumption that the control surface remains submerged for the duration of the simulation, modeling of the hydrodynamics was implemented with nonlinear lift and drag coefficients. A more detailed discussion of the control surface hydrodynamics can be found in Appendix A.2. In addition to the hydrodynamic reaction forces discussed above, ocean wave-induced disturbances can inject/remove additional energy from the control surface system. For the purposes of this study, ocean disturbances were modeled using a Pierson-Moskowitz spectrum. This model

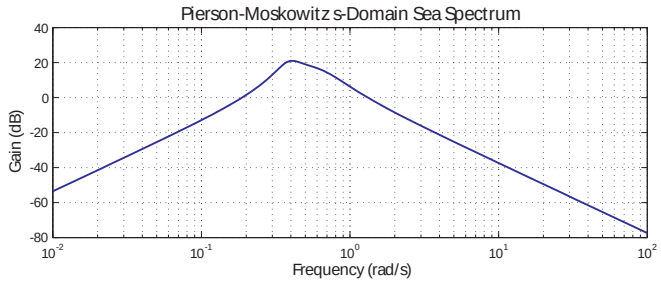

Figure 5: Frequency response due to Pierson-Moskowitz ocean spectrum.

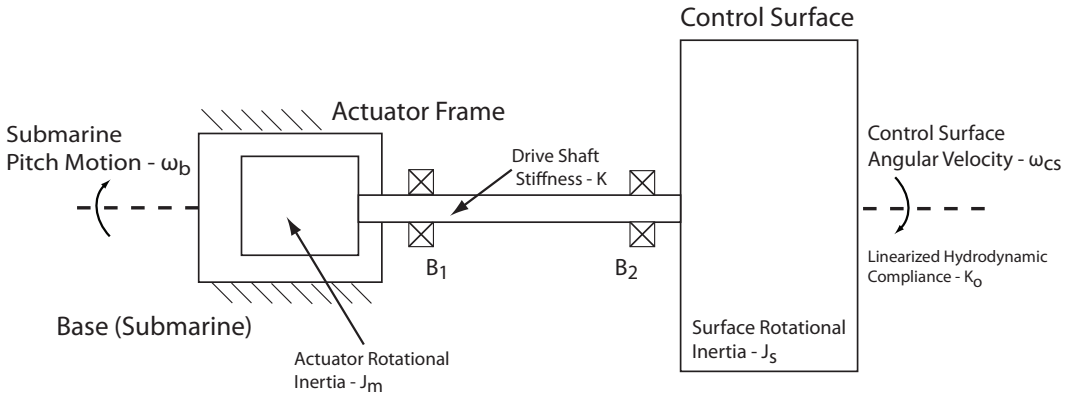

Figure 6: Simplified layout of control surface system.

was transformed via a Beaufort number relationship [7] to derive the spectrum shown in Figure 5. This spectrum was used throughout this study to model ocean disturbances. The methodology used can be applied to explore the influence of other sea states, besides that defined by a Pierson-Moskowitz spectrum.

2.3 Control Surface Actuation-Ship Interconnection

The interconnection or coupling between the control surface forces and the main ship motion requires that a specific architecture be chosen. The mechanical arrangements for submarine control surface controls can take several different forms (e.g., as described in [1]). For the purposes of this study, the somewhat idealized layout illustrated in Figure 6 was used and enabled us to experiment with key dynamic effects. Specifically, in addition to the external loading from hydrodynamic forces, the layout chosen incorporates nominal elastic, inertia, and damping effects. No specific actuator technology appears in the simplified layout of Figure 6 since a goal of this study was to formulate requirements for actuator systems that could be inserted in this space to achieve overall submarine motion requirements. The actuator system layout was modeled using bond graph methods, which are useful in modeling a very wide range of engineering system types and complexity [8]. The bond graph model of the actuator layout was useful in two ways. First, the model was readily integrated with the overall submarine model so that full system simulations could be conducted (as described

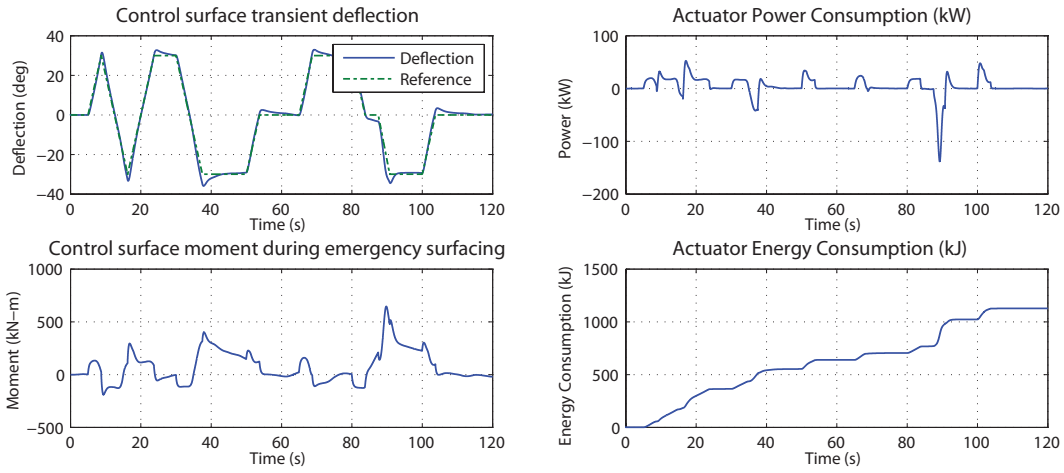

Figure 7: Dynamic demands during full sweep simulation.

later). Second, the representation of the actuator system layout in bond graph form also facilitated application of impedance methods as presented in Appendix C.2. The following sections describe how these model-based studies were conducted and used.

3 Formulating Requirements for Actuation Subsystems

Two techniques useful in retrofit design were explored in this study. First, it was shown how simulations of the full submarine can be used to derive required control surface actuator forces. For specified operational scenarios, different types of requirements can be derived. The example of finding energy requirements for extreme maneuvers is described. Secondly, it is shown how these models can be used to derive requirements in the form of impedance functions to aid design synthesis.

3.1 Energy Requirements during Extreme Maneuvering

For a typical submarine mission, the actuation systems encounter the greatest hydrodynamic torque demands during sharp yaw or pitch banks [9]. To demonstrate prediction of the dynamics of a submarine performing extreme pitch bank maneuvers, a full sweep and hold of the stern plane actuation system was simulated. This maneuver is analogous to a rapid rising and falling of the submarine during operation without a change in ballast pressure. Additionally, the ONR utilizes this basic test for the quantification of actuation systems [1]. Figure 7 displays the results of the full sweep maneuver. During the holding maneuver in Figure 8, the torque demand continues. From the persistent demand for torque actuation, the final actuation design must be capable of four quadrant operation, meaning both actuation and holding. The other simulation of interest is the emergency surfacing maneuver [1]. Unlike the continuous sweep simulation above, the control surfaces during the maneuver

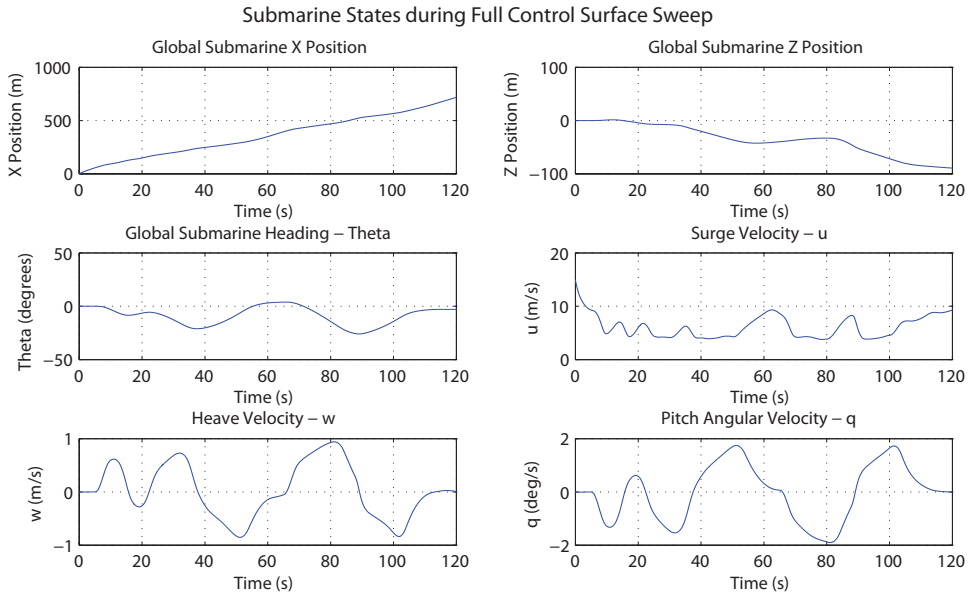

Figure 8: Selected submarine states for full sweep maneuver.

perform precision tracking to orientate the submarine to the proper global angle (θ) so that the vessel exits the water at the proper angle for structural integrity. Additionally, with the large change of buoyancy after blowing the ballast chamber, the stern plane actuators must ensure that the ascent is controlled rather than allowing the submarine system to destabilize. In the worst case, an uncontrolled ascension could exit the water perpendicularly causing bodily harm to the crew and severe damage to the structural systems. Selected states of the submarine model during the surfacing maneuver are shown in Figure 9. The submarine model states correspond closely with previous submarine modeling studies, such as [5]. Power flow analysis during the emergency surfacing maneuver helps quantify power and energy consumption requirements. Results from this type of simulation study are summarized in Figure 10.

3.2 Disturbance Rejection Requirements

Simulation of extreme maneuvers provides information on the requirements for both the power demands of the actuator and the local energy requirements for various maneuvers. These results can be used directly by domain experts to build specifications for new actuator systems. For a synthesis of design candidates from simulation data, other techniques can be applied [10]. To illustrate, another simulation study was constructed examining rejection of ocean disturbances by using the control surface actuators. For this case, the actuator package dynamics were studied only locally (i.e., the full submarine model was not needed) with imposed hydrodynamic loads. The results derived are the nominal system response characteristics shown in Figure 11. The two-port detailed derivation of this frequency domain model, including hydrodynamic Hoerner linearization, is provided in Appendix A.2. Superimposing the Pierson-Moskowitz ocean disturbance spectrum (see Figure 12) illustrates the hypothetical energy cost of rejecting disturbances with an actuator system that is purely

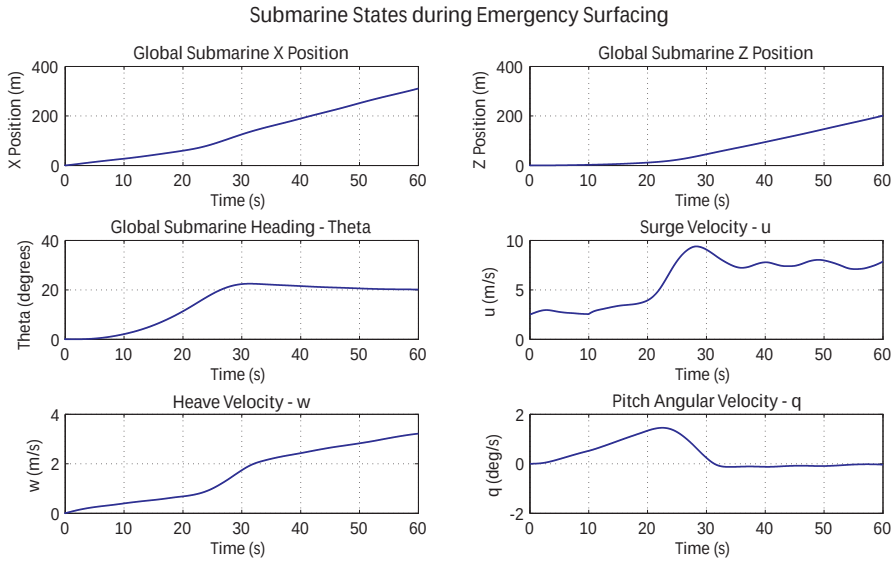

Figure 9: Selected submarine states for rapid ascension maneuver.

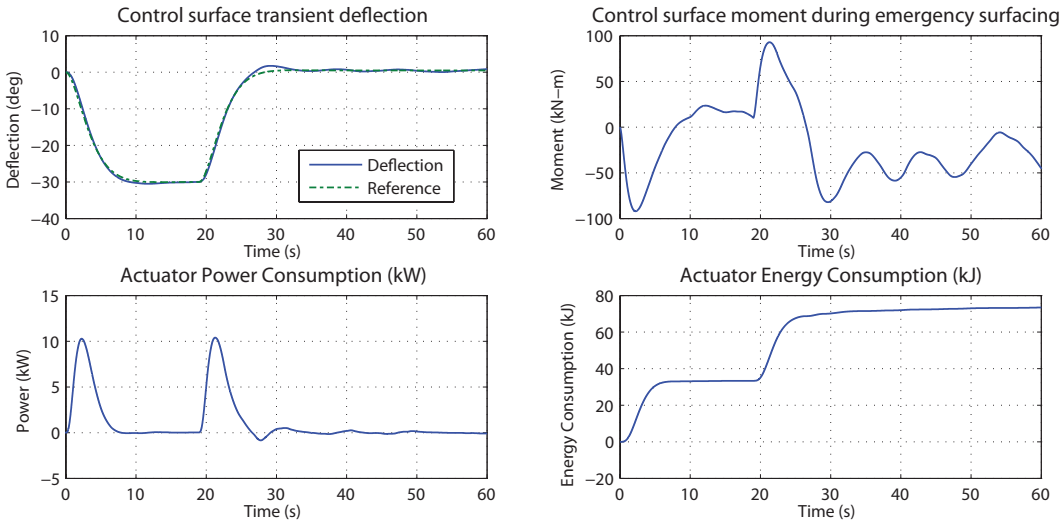

Figure 10: Control surface deflection and dynamic demands during emergency surfacing.

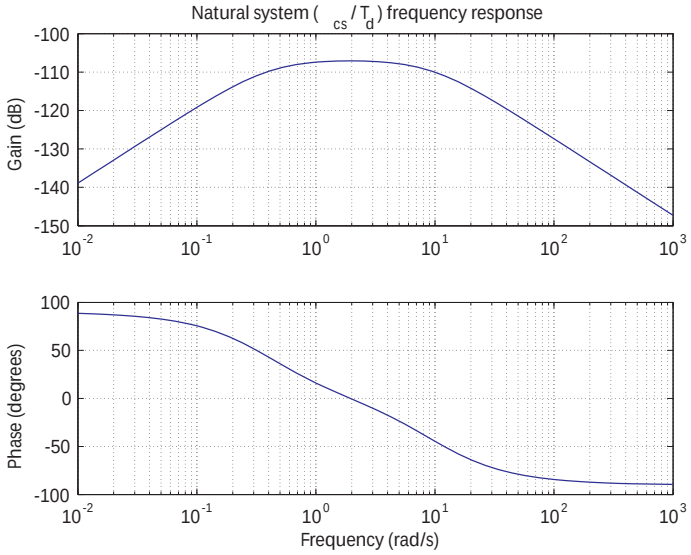

Figure 11: Command-hold frequency response of control surface system.

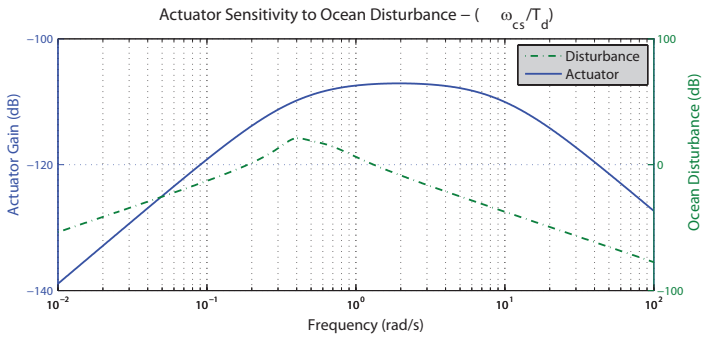

Figure 12: Pierson-Moskowitz normalized to the Control surface System Response.

active; i.e., the disturbance forces are counter-acted entirely by the powered actuator. As shown, the magnitude of the response remains high in this frequency band, so energy is sapped from the system and power required for disturbance rejection increases. It will be illustrated in section 4.2 that a two-port impedance synthesis method allows us to recommend an alternative actuator system design that can passively reject these disturbances. As such, these methods provide a designer with alternative options for addressing the various requirements, such as disturbance rejection, that may need to be considered during the actuator system retrofit process.

4 Retrofit Design via Specified Requirements

The following is a demonstration of ways for generating design candidates given system requirements derived from the simulation models previously discussed.

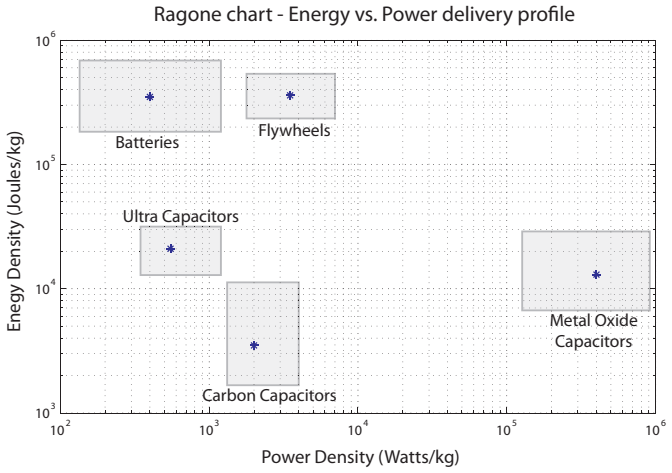

Figure 13: Comparison of energy density to power density of energy storage devices [12].

4.1 Ragone chart design of energy storage

With the estimated energy requirements for extreme maneuvers from Section 3.1, energy storage devices can be sized accordingly [4, 11]. One commonly used methodology, albeit *ad hoc*, is technology identification through a Ragone chart. For storage of energy needed to power an electromechanical actuation system, many suitable technologies exist [12]. Figure 13 shows many of the potential energy storage technologies that could provide emergency power and regulate the voltages provided to the system electronics. The energy consumption predicted via simulation for the single actuator can support systematic selection and sizing of energy storage requirements. A summary of the key simulation results is given in Table 2. In the event of power failure, additional energy may also be needed in case actuations are incomplete. An askew control surface, for example, could potentially drive the entire submarine system into a state of instability. For a single actuator, the energy storage should be five times the encountered peak for an extension to the amount of time a maneuver could persist [13]. The resulting predicted energy storage required is 2465 kJ. Given the simulation

Table 2: Fundamental Simulation Results for Single Actuator

Full Sweep	
Peak Power	130 kW
Total Energy	493 kJ
Emergency Surfacing	
Peak Power	10 kW
Total Energy	80 kJ

results, *ad hoc* energy storage and actuator system sizing is possible [12]. Identification of viable storage technologies can be accomplished using the Ragone chart in Figure 13. The energy storage mechanism must contain a large energy density in comparison to the relative power density of the system. These are preliminary results, and further investigation into the preferred energy storage for submarine applications should be conducted.

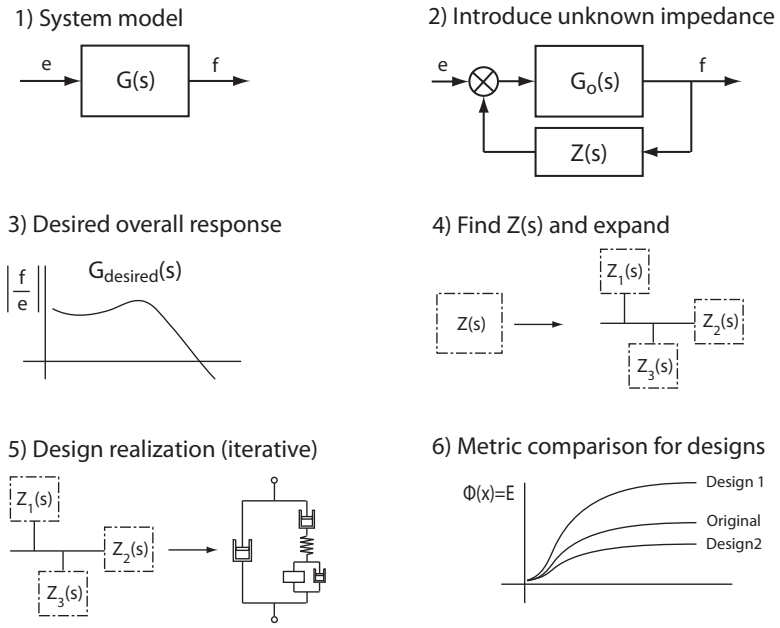

Figure 14: Flowchart of synthesis procedure.

The placement of the energy storage device in the system topology also remains heuristical [4, 12]. A potential design could have the energy storage in a centralized location much akin to the current hydraulic accumulator designs [9]. However, centralized energy storage requires power transport and distribution that add losses to the system [14]. Another possibility is to have localized energy storage for each actuation system. This setup provides quick response times but once the power in one area is exhausted, energy from other underutilized actuators proves difficult to relocate quickly to drained systems in the event of power failure [15]. Also note that the voltage type of the ship power grid is also a crucial factor [1].

While the *ad hoc* design methodology produces feasible designs, the topology and energy storage mechanisms are not necessarily ideal for the submarine system. Completion of the design process requires expert and/or *a posteriori* knowledge of energy systems as well as the submarine specific application. The system simulations provide insight into actuation energy requirements for physical submarine maneuvers which aid in energy storage sizing.

4.2 Retrofit Actuator Design via Impedance Methods

In the following, the synthesis approach is shown to produce not only the required energy storage for a given actuation task, but also potential designs for the energy storage mechanism. Rather than heuristical placement of components in a given system, a direct identification of both component location and size is found [16, 17]. Two-port impedance synthesis requires less direct involvement from system experts and allows for novel design candidate generation [18]. The steps in this procedure are summarized in Figure 14. For retrofit design generation in the case of the submarine actuation system, we reformulate the notional multi-domain (bond graph) model to incorporate a two-port black box (see Figure 15). With the goal of

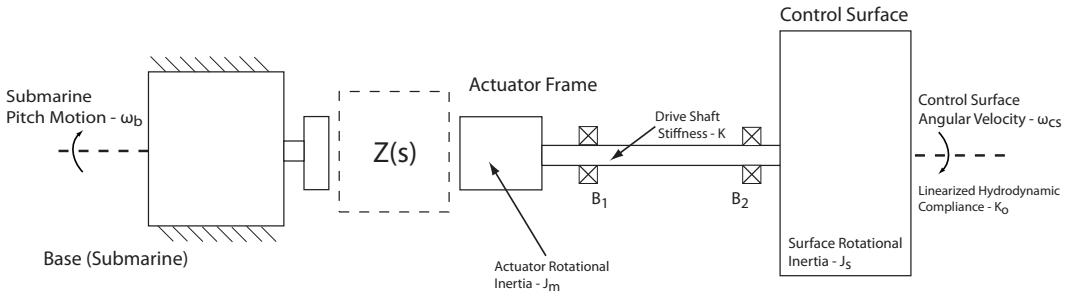

Figure 15: Two-port modification of notional system.

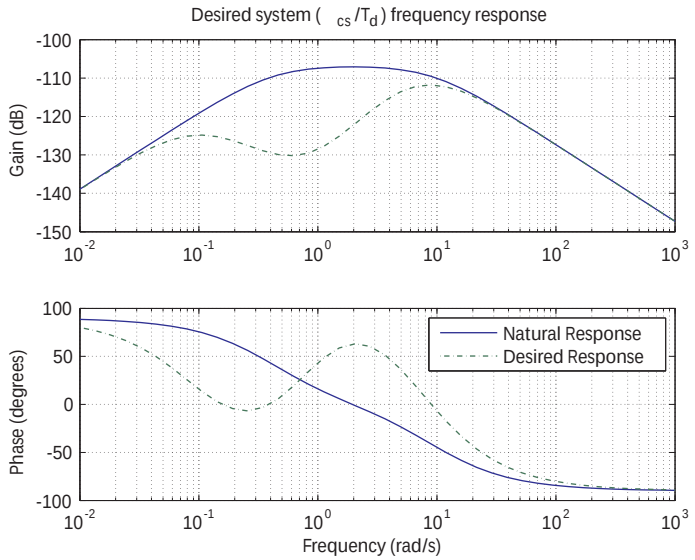

Figure 16: Adjusted desired response of system.

rejecting disturbances having frequency content described by a Pierson-Moskowitz spectrum, a desired hold-command response can be adjusted. Attenuation of disturbance frequencies in the band of the Pierson-Moskowitz spectrum becomes a new desired system response, as seen in Figure 16. Executing the synthesis methodology with the given system and desired response produces a two-port impedance function, Z(s) [10]. Converting $Z(s)$ to a real system can prove to be problematic, as discussed in Appendix C.2. Typically the form of the $Z(s)$ function makes it difficult to formulate a physical realization, especially in the face of uncertainty [19]. Additionally, the resulting impedance function, $Z(s)$, contains both active components and passive components. The active components of $Z(s)$ can be implemented through the actuator as feedback as illustrated in Figure 17. However, order reduction (balanced realization) on the system can lead to a good approximation of the system as shown in Figure 18. This approximate function form of $Z(s)$ can lead to a more realistic, simplified system realization. The order reduction in this case removes the need for high order active components [19]. As a result, the actuation system can reject ocean disturbances passively. The basic structure of this design is shown in Figure 19. Interestingly, the result of using an impedance synthesis methodology is a design which contains a local energy storage device. This energy storage mechanism recharges using power from ocean disturbances. The system

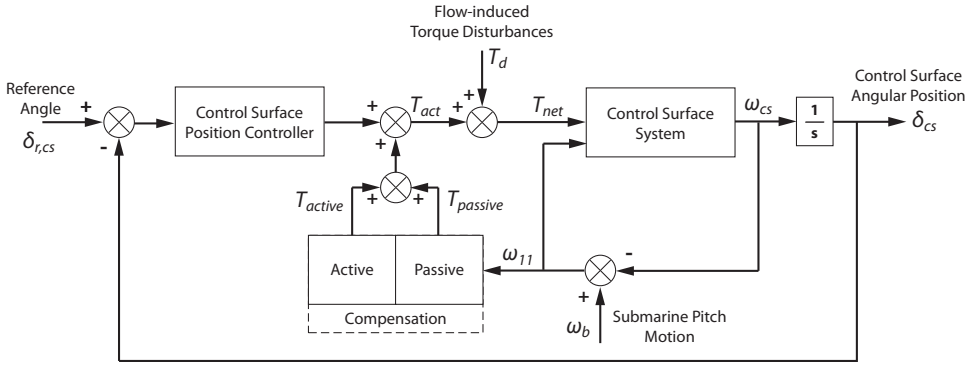

Figure 17: Block diagram representation of $Z(s)$.

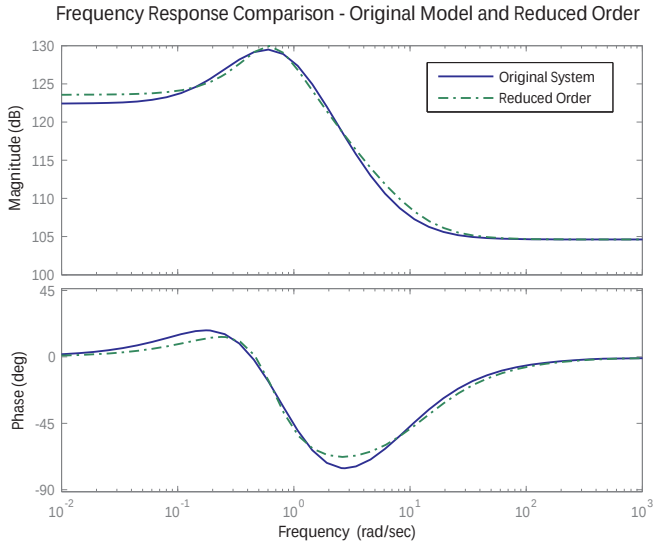

Figure 18: Model order reduction for design realization.

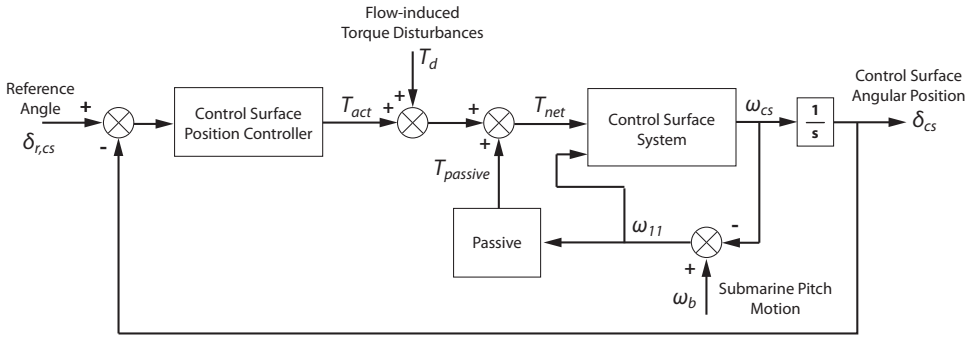

Figure 19: Block diagram representation of purely passive ocean rejection system.

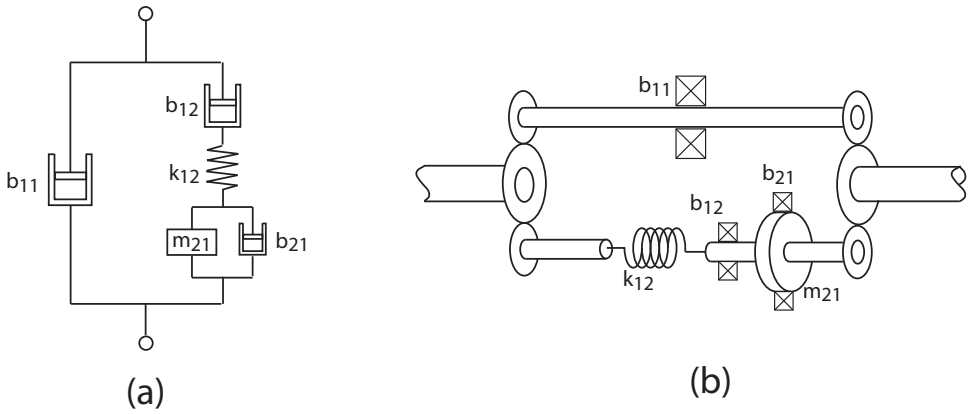

Figure 20: (a) Linear mechanical realization of reduced impedance function. (b) One potential rotational realization of the reduced impedance.

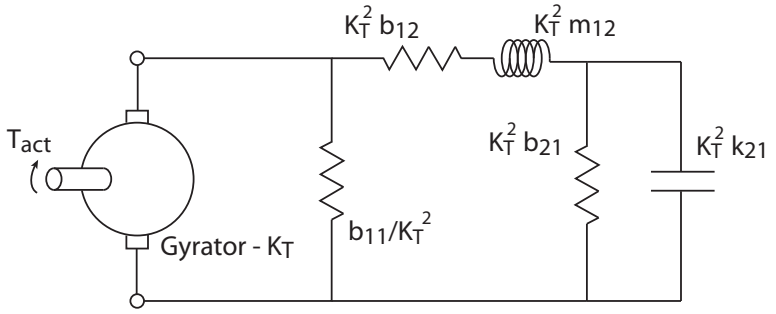

Figure 21: Electrical schematic of electrical compensation function.

rejects external energy by storing it locally in a notional capacitive element. As shown by Figure 20, this energy storage mechanism can be realized in alternative energy domains; i.e., using different technological insertions. In the case of this design process, the push towards an integrated electrical power system may suggest that Figure 21 would produce a preferred storage mechanism.

5 Conclusions

Both the simulation-based and impedance-based synthesis techniques developed in this work are viable approaches for aiding early-stage design and/or retrofit of actuator subsystems. The full system model simulations can be used to study various operational maneuvers so that actuation system requirements can be formulated directly. Synthesis techniques can employ relatively basic system models and can be useful, especially in light of a limited knowledge base, in providing alternative design configurations. Both approaches and results are reported in more detail in [10, 19, 15, 14].

In the applications examined, the synthesis approaches lead to compensating effects for

actuators. Nevertheless, it was demonstrated that the resulting designs could lead to a notable reduction in energy consumption for systems with identical power density. This suggests that the synthesis methods can help guide how passive and/or active topologies for energy storage might be combined when designing and/or retrofitting actuation subsystems.

References

[1] "ONR BAA Announcement Number 09-011," Tech. Rep. Number 09-011, 2008.

[2] H. Stevens, "Electric warship science and technology: A summary of onr 334 planning information," Tech. Rep. MSD-50-TR-2002/23, 2002.

[3] "Hydraulic v. electrical power for deepwell cargo pump systems," tech. rep., Deltamarine for Hamworthy KSE.

[4] B. Stafford and N. Osborne, "Technology development for steering and stabilizers," *Journal of Engineering for Maritime Environment*, vol. Vol. 222, No. 2, pp. 41–52, 2008.

[5] G. D. Watt, "Modelling and simulating unsteady six degrees-of-freedom submarine rising maneuvers," tech. rep., Defence Research and Development Canada - Atlantic, 2007.

[6] N. Manring, *Hydraulic control systems*. Hoboken, NJ: John Wiley & Sons, 2005. Page 58 of notes.

[7] C. K. Li and J. R. Leigh, "S-domain realisation of sea spectrum," *Electronics Letters*, vol. 19, no. 5, 1983.

[8] D. C. Karnopp, D. L. Margolis, and R. C. Rosenberg, *System Dynamics: Modeling and Simulation of Mechatronic Systems*. John Wiley & Sons, Inc., New York, 2001.

[9] R. Burcher and L. Rydill, *Concepts in Submarine Design*. Ocean Technology, Cambridge: Cambridge University Press, 1994.

[10] J. R. LeSage, *Electromechanical Retrofit of Submarine Control Surface Actuators*. PhD thesis, The University of Texas at Austin, 2010.

[11] D. P. Rubertus, L. D. Hunter, and G. J. Cecere, "Electromechanical actuation technology for all-electric aircraft," *IEEE Transactions on Aerospace and Electronic Systems*, vol. 20, no. 3, p. 243, 1983.

[12] J. Jensne, *Fundamentals of energy storage*. New York: Wiley, 1984.

[13] J. D. Boskovic, S. E. Bergstrom, and R. K. Mehra, "Retrofit reconfigurable flight control in the presence of control effector damage," in *Proceedings of the 2005 American Control Conference*, vol. 4, pp. 2652 – 2657, 2005.

[14] J. R. LeSage, R. G. Longoria, and W. Shutt, "Power system stability analysis of synthesized complex impedance loads on an electric ship," in *Electric Ship Technologies Symposium (ESTS), 2011 IEEE*, pp. 34–37, 2011.

[15] R. G. Longoria, J. R. LeSage, and W. Shutt, "Modeling and requirements formulation for submarine control surface acuation systems," in *ASNE Day 2010*, April 8-9, Crystal City, Arlington, VA 2010.

[16] M. Smith, "Synthesis of mechanical networks: The inerter," *IEEE Transactions on Automatic Control*, vol. 47, no. 10, pp. 1648–1662, 2002.

[17] T. J. Connolly and R. G. Longoria, "An approach for actuation specification and synthesis of dynamic systems," *Journal of Dynamic Systems, Measurement, and Control*, vol. 131, no. 3, 2009.

[18] K. Seo, Z. Fan, J. Hu, E. D. Goodman, and R. C. Rosenberg, "Toward a unified and automated design methodology for multi-domain dynamic systems using bond graphs and genetic programming," *Mechatronics*, vol. 13, no. 8-9, pp. 851 – 885, 2003.

[19] J. R. LeSage, W. Shutt, and R. G. Longoria, "Two-port synthesis for retrofit design of electric ship control surface actuation systems," in *ASME Dynamic Systems and Control Conference*, Boston, MA, September 13-15 2010.

[20] I. H. Abbot, *Theory of wing sections, including a summary of airfoil data.* New York: Dover Publications, 1959.

[21] H. Baher, *Synthesis of Electrical Networks.* New York: John Wiley, Inc., 1984.

[22] N. Balabanian, *Network Synthesis.* New Jersey: Prentice-Hall, Inc., 1958.

[23] M. Bayard, "Synthesis of n-terminal pair network," *in Proceedings of Brooklyn Polytech. Symposium on Modern Network Synthesis*, vol. 1, pp. 66–83, 1952.

[24] J. Beaman and R. Rosenberg, "Constitutive and modulation structure in bond graph modeling," *Journal of Dynamic Systems, Measurement and Control, Transactions ASME*, vol. 110, no. 4, pp. 395–402, 1988.

[25] J. J. Beaman and H. M. Paynter, *Modeling of Physical Systems.* 1994.

[26] R. Blevins, *Applied Fluid Dynamics Handbook.* New York, NY: Van Nostrand Reinhold Company, 1984.

[27] R. Bott and R. Duffin, "Impedance synthesis without use of transformers," *Journal of Applied Physics*, vol. 20, p. 816, 1949.

[28] O. Brune, "Synthesis of finite two-terminal network whose driving point impedance is a prescribed function of frequency," *Journal of Mathematics and Physics*, vol. 10, pp. 191–236, 1931.

[29] J. R. Carstens, *Automatic Control Systems and Components.* Englewood Cliffs, NJ: Prentice Hall, 1990.

[30] W. Cauer, *Synthesis of Linear Communication Networks*. New York: McGraw-Hill Book Company, 1958.

[31] P. M. Chirlian, *Integrated and Active Network Synthesis*. Prentice-Hall, Englewood Cliffs, New Jersey, 1967.

[32] T. J. Connolly, *Synthesis of Multiple-Energy Active Elements for Mechanical Systems*. PhD thesis, Department of Mechanical Engineering, The University of Texas at Austin, 2000.

[33] J. Feldman, "Dtnsrdc revised standard submarine equations of motion," tech. rep., Naval Ship Research and Development Center, 1979.

[34] T. I. Fossen, *Guidance and Control of Ocean Vehicles*. Chichester: John Wiley & Sons., 1994.

[35] R. Foster, "Theorems on the driving point impedance of two-mesh circuits," *Bell Systems Technology Journal*, vol. 3, p. 651, 1924.

[36] G. Fronista and G. Bradbury, "An electromechanical actuator for a transport aircraft spoiler surface," in *Proceedings of the 32nd Intersociety Energy Conversion Engineering Conference (IECEC-97)*, vol. 1, pp. 694 –698, July-August 1997.

[37] P. Gawthrop and L. Smith, *Metamodelling: For bond graphs and dynamic systems*. Series in Systems and Control Engineering, London: Prentice Hall, 1996.

[38] M. Gertler and G. R. Hagen, "Standard equations of motion for submarine simulation," tech. rep., Naval Ship Research and Development Center, June 1967 1967.

[39] D. Hazony, *Elements of Network Synthesis*. New York: Reinhold Publishing Corp., 1963.

[40] A. J. Healey and D. Lienard, "Multivariable sliding-mode control for autonomous diving and steering of unmanned underwater vehicles," *IEEE Journal of Oceanic Engineering*, vol. 18, no. 3, pp. 327–339, 1993.

[41] S. Hoerner, *Fluid Dynamic Drag*. Hoerner Fluid Dynamics, 1993.

[42] J. Hu, E. Goodman, and R. Rosenberg, "Topological search in automated mechatronic system synthesis using bond graphs and genetic programming," in *Proceeding of the 2004 American Control Conference*, vol. 6, pp. 5628–5634, June 30-July 2, Boston, MA, 2004.

[43] L. P. Huelsman, *Circuits, Matrices, and Linear Vector Spaces*. McGraw-Hill Electronic Sciences Series, New York: McGraw-Hill Book Company, Inc., 1963.

[44] R. Isermann, "Modeling and design methodology for mechatronic systems," *Mechatronics, IEEE/ASME Transactions on*, vol. 1, no. 1, pp. 16–28, 1996.

[45] T. M. Josserand, *Optimally-Robust Nonlinear Control of a Class of Robotic Underwater Vehicles*. PhD thesis, 2006.

[46] D. Karnopp, "Active and semi-active vibration isolation," *Transactions of the ASME Journal of Mechanical Design*, vol. 117B, pp. 177–185, 1995.

[47] D. Karnopp, "Power requirements for vehicle suspension systems," *Vehicle System Dynamics*, vol. 21, no. 1, pp. 65–71, 1992.

[48] D. Karnopp and R. C. Rosenburg, *Analysis and Simulation of Multiport Systems*. Cambridge, Massachusetts: The MIT Press, 1968.

[49] G. R. Keller, *Hydraulic system analysis*. Hdraulics and Pneumatics Magazine, 1969.

[50] S. Kim, *A Bond Graph Approach to Analysis, Synthesis and Design of Dynamic Systems*. PhD thesis, Department of Mechanical Engineering, The University of Texas at Austin, 2003.

[51] A. Larky, "Negative-impedance converters," *Circuit Theory, IRE Transactions on*, vol. 4, no. 3, pp. 124–131, 1957.

[52] E. V. Lewis, *Motions in waves and controllability*, vol. 3 of *Principles of naval architecture*. Jersey City: The Society of Naval Architects and Marine Engineers, 1988.

[53] S. Liu, L. Fang, and J.-l. Li, "Rudder/flap joint intelligent control for ship course system," in *IEEE International Conference on Mechatronics and Automation*, (Harbin, China), pp. 1890–1895, 2007.

[54] D. Margolis, "Energy regenerative actuator for motion control with application to fluid power systems," *Journal of Dynamic Systems, Measurement, and Control*, vol. 127, pp. 33–40, 2005.

[55] E. W. McGookin and D. J. Murray-Smith, "Submarine manoeuvring controllers optimisation using simulated annealing and genetic algorithms," *Control Engineering Practice*, vol. 14, pp. 1–15, 2006.

[56] H. E. Merritt, *Hydraulic control systems*. New York: Wiley, 1967.

[57] A. F. Molland and S. R. Turnock, *Marine Rudders and Control Surfaces*. Oxford: Elsevier Ltd., 2007.

[58] B. Moore, "Principal component analysis in linear systems: Controllability, observability, and model reduction," *IEEE Transactions on Automatic Control*, vol. 26, pp. 17–32, 1981.

[59] B. R. Munson, D. F. Young, and T. H. Okiishi, *Fundamentals of Fluid Mechanics*. John Wiley & Sons, Inc., 5th ed., 2006.

[60] R. W. Newcomb, *Linear Multiport Synthesis*. McGraw-Hill Book Company, Inc., New York, 1966.

[61] R. F. Ngwompo, S. Scavarda, and D. Thomasset, "Inversion of linear time-invariant siso systems modelled by bond graph," *Journal of the Franklin Institute*, vol. 333, no. 2, pp. 157–174, 1996.

[62] J. S. Park and J. S. Kim, "Dynamic system synthesis in terms of bond graph prototypes," *KSME International Journal*, vol. 12, no. 3, pp. 429–440, 1998.

[63] D. L. Paster, "Importance of hydrodynamic considerations for underwater vehicle design," *IEEE Journal of Oceanic Engineering*, 1986.

[64] H. M. Paynter, *Analysis and Design of Engineering Systems*. The MIT Press, 1960.

[65] W. J. Pierson and L. Moskowitz, "A proposed spectral form for fully developed wind seas based on the similarity theory," tech. rep., New York University, 1963.

[66] R. Pintelon and J. Schoukens, *System Identification: A Frequency Domain Approach*. New York: IEEE Press, 2001.

[67] T. Prestero, "Development of a six-degree of freedom simulation model for the remus autonomous underwater vehicle," tech. rep., Office of Naval Research, 2002.

[68] R. Redfield and B. Mooring, "Concept generation in dynamic systems using bond graphs," *ASME Winter Annual Meeting symposium*, vol. 8, 1988.

[69] R. C. Redfield, "Bond graphs as a tool in mechanical system conceptual design," *Automated Modeling*, vol. 41, 1992.

[70] R. C. Redfield, "Configurational design of an internal velocity sensor using bond graphs," *Advances in Instrumentation*, vol. 30, 1991.

[71] R. Rosenberg, E. Goodman, and K. Seo, "Some key issues in using bond graphs and genetic programming for mechatronic system design," in *Proceeding of ASME International Mechanical Engineering Congress and Exposition*, vol. 70, (New York, NY), pp. 355–362, 2001.

[72] R. Rosenberg and D. Karnopp, *Introduction to Physical System Dynamics*. McGraw-Hill Book Co., Inc., New York, 1983.

[73] E. Rossingnal and J. L. Hennolter, "Kinematical and dynamical control of robotic manipulators," tech. rep., Universite Libre de Bruxelles.

[74] K. Seo, E. D. Goodman, and R. C. Rosenberg, "Design of air pump system using bond graph and genetic programming method," in *Proceedings of the 2005 Conference on Genetic and Evolutionary Computation*, (Washington, D.C.), pp. 2215–2216, 2005.

[75] M. C. Smith, "Achievable dynamic response for automotive active suspensions *," *Vehicle System Dynamics*, vol. 24, no. 1, pp. 1–33, 1995.

[76] M. C. Smith and G. W. Walker, "Performance limitations and constraints for active and passive suspensions: a mechanical multi-port approach," *Vehicle System Dynamics*, vol. 33, no. 3, pp. 137–168, 2000.

[77] K. L. Su, *Active Network Synthesis*. McGraw-Hill Book Company, 1965.

[78] G. Szita and C. K. Sanathanan, "Model matching controller design for disturbance rejection," *J. Franklin Institution*, vol. 333, no. 5, pp. 747–772, 1996.

[79] G. C. Temes and J. W. LaPatra, *Introduction to Circuit Synthesis and Design*. New York: McGraw-Hill Book Company, 1977.

[80] Y. Ting-Jen, "Controller synthesis using bond graphs," in *Proceedings of the 2001 American Control Conference*, vol. 6, pp. 4765–4770, 2001.

[81] M. S. Triantafyllou and F. S. Hover, "Maneuver and control of marine vehicles," 2003.

[82] M. V. d. Wall, P. Philips, and B. d. Jager, "Actuator and sensor selection for an active vehicle suspension aimed at robust performance," *International Journal of Control*, vol. 70, no. 4, pp. 703–720, 1998.

[83] G. D. Watt, "Estimates for the added mass of a multi-component deeply submerged vehicle," tech. rep., Defence Research and Development Canada - Atlantic, October 1988.

[84] P. Welch, "The use of fast fourier transform for the estimation of power spectra: A method based on time averaging over short, modified periodograms," *IEEE Transactions on Audio Electroacoustics*, vol. AU-15, pp. 70–73, 1967.

[85] J. Wyatt, L. Chua, J. Gannett, I. Goknar, and D. Green, "Energy concepts in the state-space theory of nonlinear n-ports: Part ii - losslessness," *IEEE Transactions on Circuits and Systems*, vol. 29, no. 7, pp. 417–430, 1982.

[86] J. Wyatt, L. Chua, J. Gannett, I. Goknar, and D. Green, "Energy concepts in the state-space theory of nonlinear n-ports: Part i-passivity," *IEEE Transactions on Circuits and Systems*, vol. 28, no. 1, pp. 48–61, 1981.

[87] *USS Pampanito - Hydraulic System*. 2009.

A Modeling and Simulation of Submarine System

In this appendix, the time-invariant nonlinear submarine vehicular kinematics and dynamics are introduced. For the sake of the reader, the equations are partially derived to reveal the framework of the submarine motion and forces. Additionally, a complete presentation of all of the equations with definitions of every term can be found in Gertler [38] and Feldman [33] and a comprehensive derivation of all of the equations can be found in Watt [5, 83]. The notation of derivation follows that of Fossen [34] with some modifications.

A.1 Mathematical Modeling of Submarine Vehicular Dynamics

By establishing simple coordinate frame relationships, the overall complexity of a six degree of freedom (DOF) model can be reduced to the least complex nonlinear form. The position and orientation of the submarine are relative to the earth-fixed frame and the linear and angular velocities are relative to the body-fixed frame. Representing these expressions in terms of vectors, the system state variables are η and ν and the forces and moments are τ as illustrated by equation (2).

$$\begin{aligned} \eta &= \begin{bmatrix} x & y & z & \varphi & \theta & \psi \end{bmatrix}^T \\ \nu &= \begin{bmatrix} u & v & w & p & q & r \end{bmatrix}^T \\ \tau &= \begin{bmatrix} X & Y & Z & K & M & N \end{bmatrix}^T \end{aligned} \tag{2}$$

The velocity vector of the earth-fixed frame and the velocities of the submarine fixed reference frame are related by equation (3).

$$\dot{\eta} = J(\eta)\nu \tag{3}$$

where J(η) is the rotation matrix expressed as equation (4).

$$J(\eta) = \begin{bmatrix} J_1(\eta_2) & 0_{3\times3} \\ 0_{3\times3} & J_2(\eta_2)] \end{bmatrix} \tag{4}$$

The subordinate matrices $J_1(\eta_2)$ and $J_2(\eta_2)$ are given by equation (5) and equation (6), respectively.

$$J_1(\eta_2) = \begin{bmatrix} \cos\psi\cos\theta & J_{12}(\eta_2) & J_{13}(\eta_2) \\ \sin\psi\cos\theta & J_{22}(\eta_2) & J_{23}(\eta_2) \\ -\sin\theta & \cos\theta\sin\varphi & \cos\theta\cos\varphi \end{bmatrix} \tag{5}$$

$$J_2(\eta_2) = \begin{bmatrix} 1 & \sin\varphi\tan\theta & \cos\varphi\tan\theta \\ 0 & \cos\varphi & -\sin\varphi \\ 0 & \sin\varphi/\cos\theta & \cos\varphi/\cos\theta \end{bmatrix} \tag{6}$$

where the remaining components of matrix (5) are given by equation (7).

$$\begin{aligned} J_{12}(\eta_2) &= -\sin\psi\cos\varphi + \cos\psi\sin\theta\sin\varphi \\ J_{13}(\eta_2) &= \sin\psi\sin\varphi + \cos\psi\cos\varphi\sin\theta \\ J_{22}(\eta_2) &= \cos\psi\cos\varphi + \sin\varphi\sin\theta\sin\psi \\ J_{23}(\eta_2) &= -\cos\psi\sin\varphi + \sin\theta\sin\psi\cos\varphi \end{aligned} \tag{7}$$

A.1.1 Nonlinear Dynamics

Combining terms from the expansion of the Lagrange equations, the rigid-body dynamics of the submarine are denoted by equation (8).

$$M_b\dot{\nu} + C_b(\nu)\nu = \tau \tag{8}$$

where the vector ν represents how the equation is defined with respect to the body. The rigid-body inertia matrix, M_b, is defined in equation (9). C_b represents the centripetal and Coriolis portions of the inertial matrix displayed in equation (10).

$$M_b = \begin{bmatrix} m & 0 & 0 & 0 & mz_G & -my_G \\ 0 & m & 0 & -mz_G & 0 & mx_G \\ 0 & 0 & m & my_G & -mx_G & 0 \\ 0 & -mz_G & my_G & I_x & -I_{xy} & -I_{xz} \\ mz_G & 0 & -mx_G & -I_{yx} & I_y & -I_{yz} \\ -my_G & mx_G & 0 & -I_{zx} & -I_{zy} & I_z \end{bmatrix} \tag{9}$$

where m is the mass of the submarine, I is moment of inertia (or correspondingly, the product of inertia) with respect to a rotation axis, x_G is the x-coordinate of the center of gravity, y_G is the y-coordinate of the center of gravity, and z_G is the z-coordinate of the center of gravity.

$$C_b(\nu) = \begin{bmatrix} 0_{3\times3} & C_{b1}(\nu) \\ -C_{b1}^T(\nu) & C_{b2}(\nu) \end{bmatrix} \tag{10}$$

$$C_{b1}(\nu) = \begin{bmatrix} m(y_Gq + z_Gr) & -m(x_Gq - w) & -m(x_Gr + v) \\ -m(y_Gp + w) & m(z_Gr + x_Gp) & -m(y_Gr - u) \\ -m(z_Gp - v) & -m(z_Gq + u) & m(x_Gp + y_Gq) \end{bmatrix} \tag{11}$$

$$C_{b2}(\nu) = \begin{bmatrix} 0 & -I_{yz}q + I_zr & I_{yz}r - I_yq \\ I_{yz}q - I_zr & 0 & -I_{xz}r + I_xp \\ -I_{yz}r + I_yq & I_{xz}r - I_xp & 0 \end{bmatrix} \tag{12}$$

Due to the components of vector ν in the Coriolis/centripetal term which couple with other terms in the ν vector, the dynamics of the submarine are nonlinear. Also note that the C_b matrix is in skew-symmetric form.

A.1.2 Restoring Forces and Control Inputs

Since the buoyancy and the weight forces act due to the orientation of the submarine to the earth-fixed frame, a transformation between the earth-fixed frame and the body frame must be preformed. Using the transformation $J_1(\eta_2)$, the restoring moments/forces coefficients are given by equation (13).

$$g(\eta) = \begin{bmatrix} (W-B)\sin\theta \\ -(W-B)\cos\theta\sin\varphi \\ -(W-B)\cos\theta\cos\varphi \\ -(y_G W - y_B B)\cos\theta\cos\varphi + (z_G W - z_B B)\cos\theta\sin\varphi \\ (z_G W - z_B B)\sin\theta + (x_G W - x_B B)\cos\theta\cos\varphi \\ -(x_G W - x_B B)\cos\theta\sin\varphi + (y_G W - y_B B)\sin\theta \end{bmatrix} \tag{13}$$

where $(x_G,\ y_G,\ z_G)$ and $(x_B,\ y_B,\ z_B)$ are the center of gravity and center of buoyancy, respectively.

The potential damping coefficients due to the skin friction are found as in Watt [83] as the integral of the viscous stress tangent to the submarine body. As in the derivation of Watt [83], the terms higher than second order are negligible and can thus be dropped. Additionally, due to the planes of symmetry of the submarine body, the damping matrices may be simplified to,

$$D(\nu) = \begin{bmatrix} D_{11}(\nu) & D_{12}(\nu) \\ 0_{3\times3} & D_{22}(\nu) \end{bmatrix} \tag{14}$$

$$D_{11}(\nu) = \begin{bmatrix} X_u + X_{u|u|}\,|u| & 0 & 0 \\ 0 & Y_v + Y_{v|v|}\,|v| & 0 \\ 0 & 0 & Z_w + Z_{w|w|}\,|w| \end{bmatrix} \tag{15}$$

$$D_{12}(\nu) = \begin{bmatrix} 0 & X_{q|q|}\,|q| & 0 \\ Y_{p|p|}\,|p| & 0 & Y_{r|r|}\,|r| \\ 0 & Y_{q|q|}\,|q| & 0 \end{bmatrix} \tag{16}$$

$$D_{22}(\nu) = \begin{bmatrix} K_p + K_{p|p|}\,|p| & 0 & K_{r|r|}\,|r| \\ 0 & M_q + M_{q|q|}\,|q| & 0 \\ Y_{p|p|}\,|p| & 0 & N_r + N_{r|r|}\,|r| \end{bmatrix} \tag{17}$$

where the first terms in the matrix are the coefficients of the skin friction factors and the second terms are the coefficients of the vortex shedding drag factors.

The force components of the control inputs can be expressed as a product of the input matrix and the input vector,

$$\tau_i = g(\nu)u_i \tag{18}$$

where $g(\nu)$ is the control parameter matrix which contains the parametric relationships of

the input vector u_i. The control parameter matrix $g(\nu)$ is,

$$g(\nu) = \begin{bmatrix} 0 & 0 & 0 & 1 \\ Y_{uu\delta_r}u^2 & 0 & 0 & 0 \\ 0 & Z_{uu\delta_s}u^2 & Z_{uu\delta_b}u^2 & 0 \\ 0 & 0 & 0 & 0 \\ 0 & M_{uu\delta_s}u^2 & M_{uu\delta_b}u^2 & 0 \\ N_{uu\delta_r}u^2 & 0 & 0 & 0 \end{bmatrix} \tag{19}$$

where the control parameters are given by the size and shape of the control surfaces. The input vector, u_i, is given as,

$$u_i = \begin{bmatrix} \delta_r \\ \delta_s \\ \delta_b \\ X_{prop} \end{bmatrix} \tag{20}$$

where δ_r is the deflection of the rudder in radians, δ_s is the deflection of the stern plane in radians, δ_b is the deflection of the bow plane in radians and X_{prop} is the simplified thrust model which only applies force in the surge direction.

A.1.3 Full Equations of Motion

By compiling the forces and moments derived in the preceding analysis, the total forces and moments on the submarine body can be found. The total inertial matrix and Coriolis/centripetal matrix can be found by summing both the body dynamics and the added mass matrices,

$$\mathrm{M} = \mathrm{M_v} + \mathrm{M_b} \tag{21}$$

$$\mathrm{C} = \mathrm{C_v} + \mathrm{C_b} \tag{22}$$

Combining these two summations with the total damping matrix, $D(\nu)$, the total force/moment on the submarine body with respect to the body frame is,

$$M\dot{\nu} + C(\nu)\nu + D(\nu)\nu + g(\eta) + g(\nu)u_i = \tau \tag{23}$$

Nevertheless, the analysis of the motion of the submarine with respect to the earth-fixed frame is of ultimate interest, so use the translation derived in equation (4). This transformation provides the vehicular dynamics in the earth-fixed frame,

$$M_\eta(\eta)\ddot{\eta} + C_\eta(\eta,\nu)\dot{\eta} + D_\eta(\eta,\nu)\dot{\eta} + g_\eta(\eta) + g(\nu)u_i = \tau_\eta \tag{24}$$

where,

$$M_\eta(\eta) = J^{-T}(\eta)M_{tot}J^{-1}(\eta) \tag{25}$$

$$C_\eta(\nu,\eta) = J^{-T}(\eta)\left[C_{tot}\nu - M_{tot}J^{-1}(\eta)\dot{J}(\eta)\right]J^{-1}(\eta) \tag{26}$$

$$D_\eta(\nu,\eta) = J^{-T}(\eta)D(\nu)J^{-1}(\eta) \tag{27}$$

$$g_\eta(\eta) = J^{-T}(\eta)g(\eta) \tag{28}$$

$$\tau_\eta(\eta) = J^{-T}(\eta)\tau \tag{29}$$

A.2 Derivation of Control Surface Modeling

Moments are produced due to the offset of the actuation rod to the center of pressure of the lift and drag forces. By assuming a constant center of pressure, the moment arm for the hydrodynamic forces also remains constant. Finally, the coefficient of lift for small angles of attack can be represented by the Hoerner empirical fin lift coefficient (c_h), [81],

$$c_h = \frac{1}{1.8\pi} + \frac{A_s}{\pi h_s^2} \tag{30}$$

where A_s is the surface area of the control surface and h_s is the height of the control surface. Since the deflection of the control surface is restricted to ± 30 degrees, the Hoerner angle assumption should hold in this case. Altering the equation of lift and accounting for the duality of the control surfaces leads to,

$$F_{L,m} = \rho U^2 A_s C_s \tag{31}$$

where U is the coupled body-fixed velocity function which is dependent on both coupled velocities as well as control surface angles of deflection. Expanding the coupled body-fixed velocity function and accounting for the center of pressure moment arm, the hydrodynamic moment equation is found,

$$M_f = \rho A_s C_s l_p \left[u^2\delta_s + uw + l_p uq\right] \tag{32}$$

where l_p is the moment arm to the center of pressure, δ_s is the control surface deflection, u is the surge velocity, w is the heave velocity and q is the pitch velocity. Coupled with the control surface dynamics, the hydrodynamic moments about the control surface produce the required actuation torque for both steady state and transient actions.

An interesting note on the linearized hydrodynamic moment is that the moment function behaves as a linear compliance. Combining terms to form the linearized moment compliance parameter, the function is simplified to a linear impedance element as shown by equation (33).

$$M_{f,l} = k_o\theta_s \;\; \Rightarrow \;\; k_o = \rho A_s C_s l_p u^2 \tag{33}$$

A.2.1 Control Surface and Electromechanical System Modeling

This control surface system model assumes the actuation system will couple into rotational inertia, J_m, which is connected to the control surface by a drive shaft having stiffness, K. On each end of the drive shaft, bearing losses are accounted for by linear frictional damping coefficients B_1 and B_2. The control surface is lumped as a single inertia with moment of inertia, J_s. Additionally, the linearized ocean compliance, from equation (33) is also incorporated into the two-port model as another applied torque on the control surface

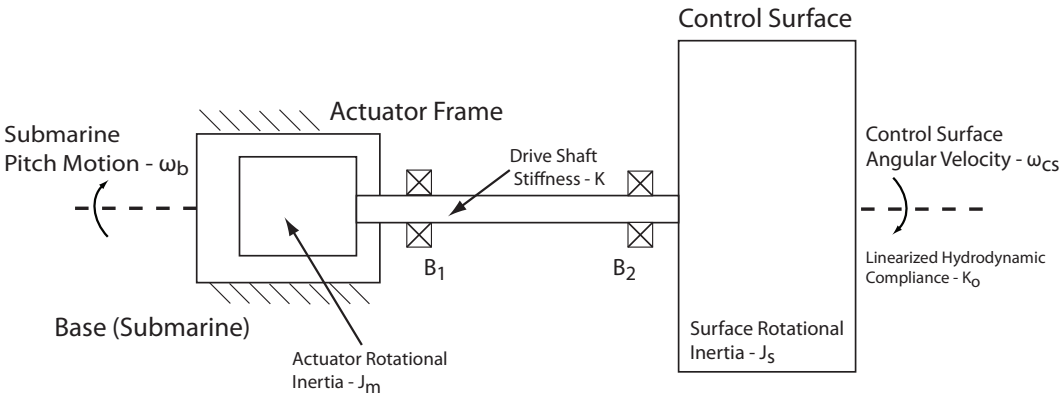

Figure 22: Simplified layout of control surface system.

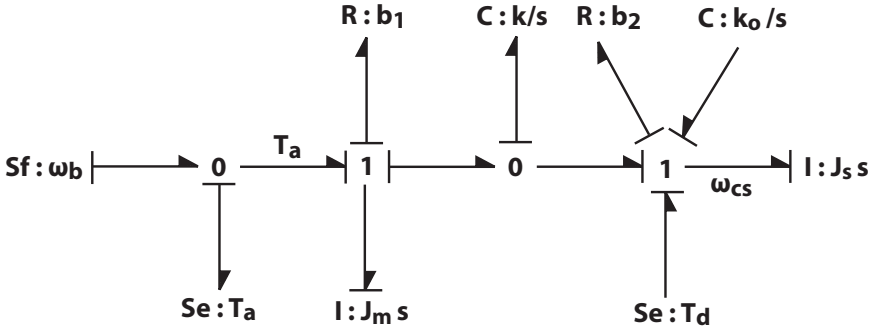

Figure 23: Bond graph form of the control surface system with ideal torque actuator.

inertia [53].

A.2.2 Bond Graph Approach for Generic Representation of Components

Since force components are assumed to be linear including the ocean hydrodynamic moments, the resulting equation is a linear ordinary differential equation. Figure 23 contains the topology of the energy flow in the control surface system in bond graph form. The state equations for the control surface system dynamics are derived using the bond graph and take the form,

$$\begin{bmatrix} \dot{h}_s \\ \dot{\theta}_s \\ \dot{h}_m \\ \dot{\theta}_k \end{bmatrix} = \begin{bmatrix} 0 & k & -b_2/J_s & k_o \\ 0 & 0 & 0 & 1/J_s \\ -b_1/J_m & -k & 0 & 0 \\ 1/J_m & 0 & -1/J_s & 0 \end{bmatrix} \begin{bmatrix} h_s \\ \theta_s \\ h_m \\ \theta_k \end{bmatrix} + \begin{bmatrix} 1 & 0 & 0 \\ 0 & 0 & 0 \\ 0 & 0 & 1 \\ 0 & 0 & 0 \end{bmatrix} \begin{bmatrix} T_d \\ \omega_b \\ T_a \end{bmatrix} \tag{34}$$

Due to the linearity of the control surface differential equation in equation (34), the differential equations can be readily expressed as a transfer function relating the input torque to

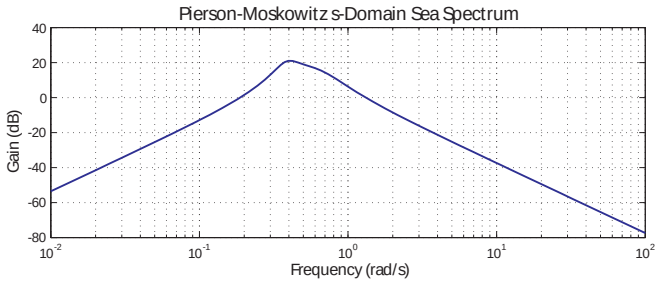

Figure 24: Magnitude of the s-domain representation of the Pierson-Moskowitz ocean spectrum.

the output surface deflection,

$$\frac{\omega_{cs}}{T_a} = \frac{s}{n_4 s^4 + n_3 s^3 + n_2 s^2 + n_1 s - k_o} \tag{35}$$

where the denominator coefficients are defined by,

$$\begin{aligned} n_4 &= \frac{J_s J_m}{k} \\ n_3 &= \frac{b_1 J_s}{k} + \frac{b_2 J_m}{k} \\ n_2 &= \frac{b_1 b_2}{k} + J_s + J_m + \frac{J_m k_o}{k} \\ n_1 &= b_1 - \frac{b_1 k_o}{k} + b \end{aligned} \tag{36}$$

A.3 Pierson-Moskowitz Spectrum

Many different models for ocean wave spectrum exist, but for the purpose of this derivation, the Pierson-Moskowitz ocean spectrum is used [65, 7]. Typically the Pierson-Moskowitz ocean spectrum is given by,

$$S(\omega) = \frac{0.0081g}{\omega^5} e^{-3.109/h_s^2 \omega^4} \tag{37}$$

where ω is the frequency in radians per second, g is the acceleration due to gravity, and h_s is the significant wave height in meters. However, since all models are derived in the s-domain, a s-domain representation of the Pierson-Moskowitz spectrum is required. A fourth order s-domain transfer function has been derived in [7] and is expressed as,

$$G(s) = \frac{K_n\, s^2}{s^4 + a_1 s^3 + a_2 s^2 + a_3 s + a_4} \tag{38}$$

where $K_n = 1.341$, $a_1 = 0.641$, $a_2 = 0.648$, $a_3 = 0.135$, and $a_4 = 0.0641$. The s-domain Pierson-Moskowitz ocean spectrum magnitude is shown in Figure 24. The ocean disturbance spectrum contains discernible torques from 0.18 rad/s to 1.25 rad/s with a peak at 0.4 rad/s. Referring back to Figure 11, the magnitude of the natural response of the control surface

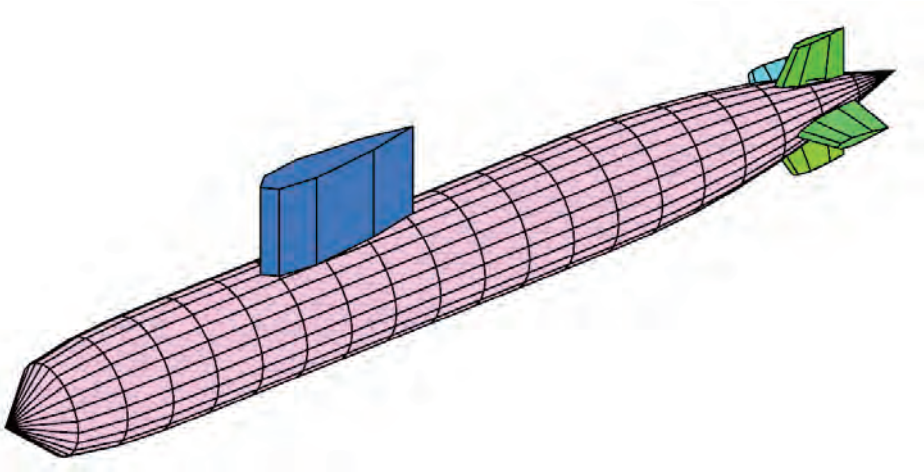

Figure 25: Model geometries used by Watt [5] to identify the rotational and mass moment derivatives.

system is near the peak in this band of frequencies.

A.4 Submarine Parameter List for Simulations

The parameters used in this report are based on the geometries of the submarine model derived by Watt [5]. However, the dimensions used throughout this report are based on the modern Virginia class submarine which has approximate dimensions given by Table 3. Parameter scaling allowed for the calculation of new mass coefficients and moments via the existing model geometries shown in Figure 25.

Table 3: Submarine Model Constant Parameters for Virginia Class Vessel

Parameter	Value	Description
l	110 m	Length of submarine
d	$l/8.75$ m	Hull diameter (semi-minor axes)
g	9.81 m/s^2	Acceleration of gravity
ρ	1010 kg/m^3	Salt water fluid density

B Synthesis Techniques Overview

In two-port systems effort, e, and flow, f, variables typically represent power variable pairs such as voltage-current, force velocity, etc. Consequently, any design problems including power transmission can be effectively modeled as an aggregate of two-port subsystems [43]. The circuit and bond graph representations of a two-port are illustratedi in Figure 26. In

Table 4: Hydrodynamic and added mass coefficients for submarine dynamics [5]

Parameter	Value	Parameter	Value	Parameter	Value
x_g	0.00	y_g	0.00	z_g	0.55
x_b	0.00	y_b	0.00	z_b	-0.55
I_{xx}	2.44×10^8	I_{yy}	8.13×10^9	I_{zz}	8.13×10^9
$X_{\dot{u}}$	-3.69×10^5	$Y_{\dot{v}}$	-1.32×10^6	$Z_{\dot{u}}$	-1.91×10^3
$X_{\dot{w}}$	-1.91×10^3	$Y_{\dot{p}}$	-2.16×10^7	$Z_{\dot{w}}$	-1.09×10^7
$X_{\dot{q}}$	6.98×10^4	$Y_{\dot{r}}$	1.52×10^6	$Z_{\dot{q}}$	-1.90×10^7
$K_{\dot{v}}$	-2.16×10^7	$M_{\dot{u}}$	6.98×10^5	$N_{\dot{v}}$	1.53×10^8
$K_{\dot{p}}$	-2.18×10^8	$M_{\dot{w}}$	-1.90×10^7	$N_{\dot{p}}$	-1.67×10^8
$K_{\dot{r}}$	-1.67×10^8	$M_{\dot{q}}$	-7.49×10^9	$N_{\dot{r}}$	-7.64×10^9
X_{uu}	1.00×10^4	Y_{vv}	2.68×10^6	Z_{ww}	2.68×10^4
X_{pp}	-2.08×10^6	X_{rr}	2.42×10^8	X_{wp}	-1.65×10^5
X_{uq}	1.28×10^4	X_{qq}	2.45×10^8	$X_{q\|q\|}$	3.70×10^4
Y_{up}	3.36×10^6	$Y_{p\|p\|}$	-1.92×10^5	Y_{ur}	7.43×10^6
$Y_{r\|r\|}$	2.29×10^8	Z_{wp}	-8.60×10^3	Z_{uq}	-8.84×10^6
$Z_{q\|q\|}$	-2.29×10^8	K_{up}	-3.13×10^7	$K_{p\|p\|}$	-1.63×10^6
K_{ur}	-1.02×10^7	$K_{r\|r\|}$	-1.63×10^6	M_{pp}	2.11×10^7
M_{rr}	2.52×10^5	M_{wp}	-2.44×10^5	M_{uq}	4.49×10^8
$M_{q\|q\|}$	-1.06×10^10	N_{up}	-4.73×10^7	$N_{p\|p\|}$	-2.44×10^6
N_{wp}	-1.83×10^6	N_{ur}	-4.77×10^8	$N_{r\|r\|}$	-1.06×10^10
$X_{\delta s \delta s}$	-1.27×10^5	$X_{\delta r \delta r}$	-1.27×10^5	$Z_{\delta s}$	-1.58×10^5
$Y_{\delta r}$	1.46×10^5	$N_{\delta r}$	-7.34×10^6	$M_{\delta s}$	-7.34×10^6
X_{vr}	$-Y_{\dot{v}}$	X_{rp}	$-Y_{\dot{p}}$	X_{wq}	$Z_{\dot{w}}$
Y_{wr}	$X_{\dot{w}}$	Y_{qr}	$X_{\dot{q}}$	Y_{wp}	$Z_{\dot{w}}$
Y_{pq}	$-Z_{\dot{q}}$	Z_{wq}	$-X_{\dot{w}}$	Z_{qq}	$X_{\dot{w}}$
X_{vp}	$-Y_{\dot{v}}$	Z_{pp}	$Y_{\dot{p}}$	Z_{rp}	$Y_{\dot{r}}$
K_{wp}	$-Y_{\dot{p}}$	K_{pq}	$K_{\dot{r}}$	K_{vq}	$Y_{\dot{r}} + Z_{\dot{q}}$
K_{wr}	$-Y_{\dot{r}} - Z_{\dot{q}}$	K_{qr}	$-M_{\dot{q}} + N_{\dot{r}}$	M_{wq}	$X_{\dot{q}}$
M_{vr}	$Y_{\dot{p}}$	M_{vp}	$-Y_{\dot{r}}$	M_{pr}	$K_{\dot{p}} - N_{\dot{r}}$
N_{qr}	$-K_{\dot{r}}$	N_{vq}	$-X_{\dot{q}} - Y_{\dot{p}}$	N_{pq}	$-K_{\dot{p}} + M_{\dot{q}}$

this body of work, the impedance synthesis technique relied exclusively on two-port systems.

B.1 Canonical Matrices

Early developers of n-port matrix theory designated certain matrix forms as "canonical". A detailed derivation of two-port matrix forms can be found in Huelsman [43] and the matrix forms are summarized in Figure 27. The synthesis methodology relies heavily on the canonical matrices and transformations between the various forms, summarized in Figure 28 [48]. Using transformation relationships, the system matrix can be defined in multiple

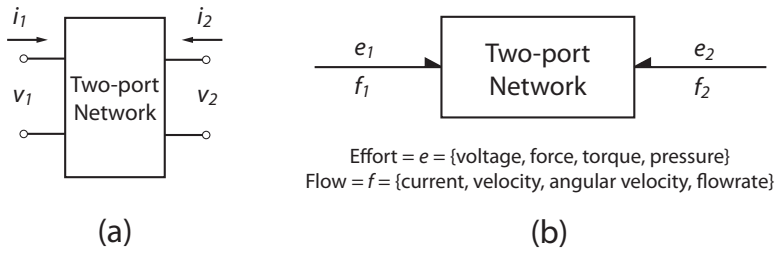

Figure 26: (a) Electrical two-port. (b) Generalized (multi-disciplinary) two-port with bonds conveying power, $P_i = e_i f_i$.

Transmission - M	$\begin{bmatrix} e_1 \\ f_1 \end{bmatrix} = \begin{bmatrix} n_{11} & \eta_{12} \\ y_{21} & n_{22} \end{bmatrix} \begin{bmatrix} e_2 \\ f_2 \end{bmatrix}$
Impedance - Z	$\begin{bmatrix} e_1 \\ e_2 \end{bmatrix} = \begin{bmatrix} \eta_{11} & \eta_{12} \\ \eta_{21} & \eta_{22} \end{bmatrix} \begin{bmatrix} f_1 \\ f_2 \end{bmatrix}$
Immittance - H	$\begin{bmatrix} e_1 \\ f_2 \end{bmatrix} = \begin{bmatrix} \eta_{11} & n_{12} \\ n_{21} & y_{22} \end{bmatrix} \begin{bmatrix} f_1 \\ e_2 \end{bmatrix}$
Adpedance - G	$\begin{bmatrix} f_1 \\ e_2 \end{bmatrix} = \begin{bmatrix} y_{11} & n_{12} \\ n_{21} & \eta_{22} \end{bmatrix} \begin{bmatrix} e_1 \\ f_2 \end{bmatrix}$
Admittance - Y	$\begin{bmatrix} f_1 \\ f_2 \end{bmatrix} = \begin{bmatrix} y_{11} & y_{12} \\ y_{21} & y_{22} \end{bmatrix} \begin{bmatrix} e_1 \\ e_2 \end{bmatrix}$

$[n] \equiv$ dimensionless

$[\eta] \equiv [e / f]$

$[y] \equiv [f / e]$

Figure 27: Two-port system canonical forms with descriptions of transfer function relationships.

Transmission - M	$\begin{bmatrix} e_1 \\ f_1 \end{bmatrix} = \begin{bmatrix} A & B \\ C & D \end{bmatrix} \begin{bmatrix} e_2 \\ f_2 \end{bmatrix}$
Impedance - Z	$\begin{bmatrix} e_1 \\ e_2 \end{bmatrix} = \frac{1}{C} \begin{bmatrix} A & -\Delta \\ 1 & -D \end{bmatrix} \begin{bmatrix} f_1 \\ f_2 \end{bmatrix}$
Immittance - H	$\begin{bmatrix} e_1 \\ f_2 \end{bmatrix} = \frac{1}{D} \begin{bmatrix} B & \Delta \\ 1 & -C \end{bmatrix} \begin{bmatrix} f_1 \\ e_2 \end{bmatrix}$
Adpedance - G	$\begin{bmatrix} f_1 \\ e_2 \end{bmatrix} = \frac{1}{A} \begin{bmatrix} C & \Delta \\ 1 & -B \end{bmatrix} \begin{bmatrix} e_1 \\ f_2 \end{bmatrix}$
Admittance - Y	$\begin{bmatrix} f_1 \\ f_2 \end{bmatrix} = \frac{1}{B} \begin{bmatrix} D & -\Delta \\ 1 & -A \end{bmatrix} \begin{bmatrix} e_1 \\ e_2 \end{bmatrix}$

Figure 28: Relationships between canonical two-port systems. Conversions are all with respect to the transmission matrix, which can be easily derived from the system bond graph.

ways allowing many different transfer function relationships to be analyzed. These system techniques have been extended to any physical domain for two-port representation. Due to the extension to multiple physical domains, the method of generating the two-port system matrices involves the use of bond graph topology.

B.2 Impedance Bond Graphs

Bond graph elements represent the basic linear or nonlinear multi-disciplinary elements of realizable systems. For those unfamiliar with bond graphs, Karnopp [8], Redfield [68, 69, 70] and Connolly [32, 17] contain overviews of the subject. Figure 29 presents a summary of the potential bond graph elements with equivalent impedances based on the causality definitions of the bond. For example, an electrical analog model for the ideal torque source, $T_a(t)$, is shown in Figure 30(a). Retrofitting the torque source, a designer can remove the known ideal torque source and replace it with an unknown impedance, $Z_a(s) = T_a/\omega_a$, shown in Figure 30(b) as electrical analog or as in (c) using an equivalent bond graph form. The synthesis methodology determines the unknown impedance function in terms of specified system response requirements.

e, f — R	$\frac{f(s)}{e(s)} = G$	e, f — I	$\frac{f(s)}{e(s)} = \frac{1}{Is}$
e, f — R	$\frac{e(s)}{f(s)} = R$	e, f — I	$\frac{e(s)}{f(s)} = Is$
e, f — C	$\frac{f(s)}{e(s)} = Cs$	e, f — n T — Z	$\frac{e(s)}{f(s)} = n^2 Z(s)$
e, f — C	$\frac{e(s)}{f(s)} = \frac{1}{Cs}$	e, f — r G — Z	$\frac{f(s)}{e(s)} = r^2 Z(s)$

Figure 29: Basic elements of bond graph notation with causal definitions. The casual definition implies the transfer function of an element.

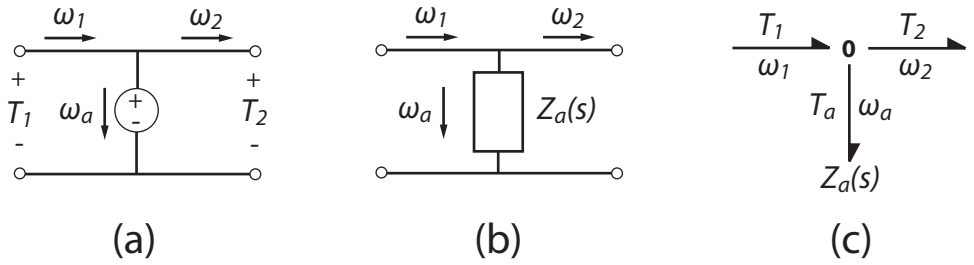

Figure 30: (a) Electrical analog for ideal torque actuation. (b) Electrical analog showing active impedance replacing torque source. (c) Bond graph form of system in (b).

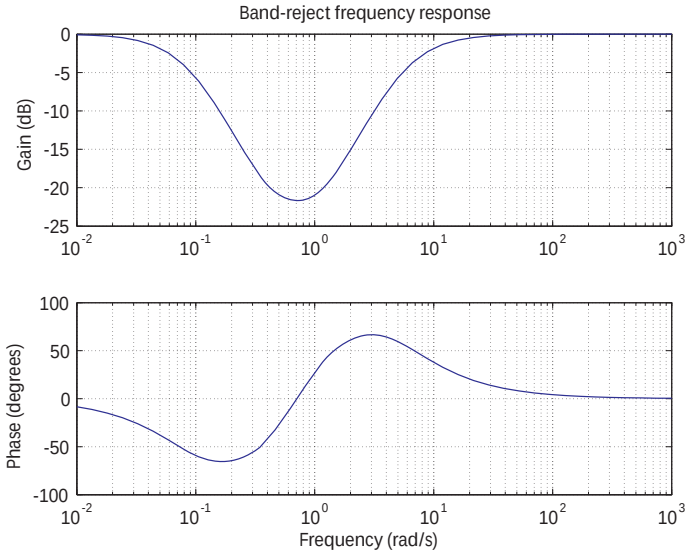

Figure 31: Band rejection response alteration to impose on the natural control surface system response.

C Derivation of Actuator Synthesis

The detailed synthesis procedure implemented on the control surface model is discussed in the following section. This process draws heavily from the theory discussed in Appendix B.

C.1 Specified Frequency Response Dynamics Derivation

To filter out ocean disturbance torques, the natural response of the system is modified to have a band reject response. This modifying function is shown in equation (39).

$$\frac{f}{e} = \left[\frac{\frac{s}{\alpha\tau_1} + 1}{\frac{s}{\tau_1} + 1} \cdot \frac{\frac{s}{\tau_2/\alpha} + 1}{\frac{s}{\tau_2} + 1} \right]^n \tag{39}$$

where $\tau_1 = 0.1$ is the lower limit of the band reject function, $\tau_2 = 5$ is the upper limit of the band reject function, $\alpha = 6$ is the slope factor, $n = 2$ is the filter order. This function has a response as shown in Figure 31. By imposing the band rejection function to the natural system response, the desired system response function is determined. Combining these functions yields equations (40).

$$dTF(s) = \frac{1}{(J_s + J_m)\, s - \frac{K_o}{s} + B_1 + B_2} \cdot \left[\frac{\frac{s}{\alpha\tau_1} + 1}{\frac{s}{\tau_1} + 1} \cdot \frac{\frac{s}{\tau_2/\alpha} + 1}{\frac{s}{\tau_2} + 1} \right]^n \tag{40}$$

Merging these functions produces a desired transfer function that will not radically alter the natural response of the system, but modifies the system to attenuate disturbance frequencies

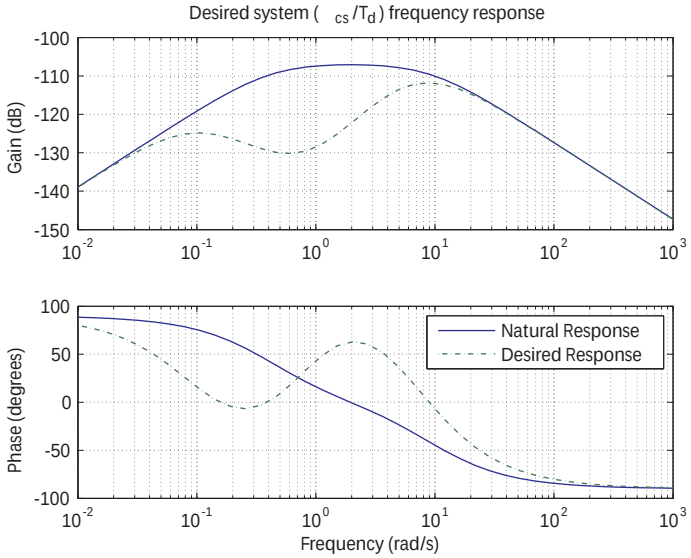

Figure 32: Comparison of the desired frequency response and the natural system response with a band rejection function.

from 0.1 rad/s to 5 rad/s. The desired frequency response which is used for the synthesis procedure is shown in Figure 32.

C.2 Submarine Actuator Two-Port Impedance

Representation of the control surface system model in bond graph topology is shown in Figure 33. Using the bond graph representation, the two-port matrices of each junction are formulated using transmission matrix form. Beginning with the right side of the bond graph model, the matrices are constructed for each element and parsed into series matrix

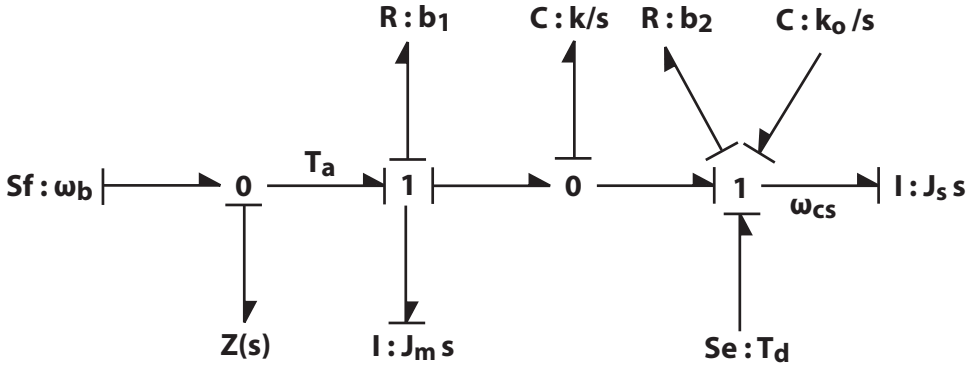

Figure 33: Bond graph representation of control surface model with specified unknown impedance function.

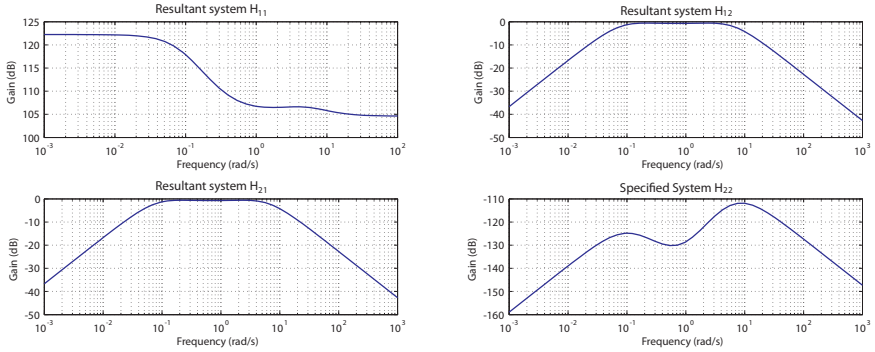

Figure 34: Comparison of the desired frequency response and the natural system response with a band reject function.

multiplication,

$$\begin{bmatrix} T_1 \\ \omega_1 \end{bmatrix} = \begin{bmatrix} 1 & 0 \\ Y_a(s) & 1 \end{bmatrix} \begin{bmatrix} 1 & B_1 + J_m s \\ 0 & 1 \end{bmatrix} \begin{bmatrix} 1 & 0 \\ s/K & 1 \end{bmatrix} \begin{bmatrix} 1 & B_2 + J_s s - K_o/s \\ 0 & 1 \end{bmatrix} \begin{bmatrix} T_d \\ \omega_{cs} \end{bmatrix} \tag{41}$$

For this derivation, the drive shaft stiffness K is allowed to approach infinity. This assumption simplifies the control surface model by eliminating high frequency harmonics from the drive shaft compliance. From the series of element junctions, the impedance function that represents the entire two-port system is calculated. The total function is represented by equation 42.

$$\begin{bmatrix} T_1 \\ \omega_1 \end{bmatrix} = \begin{bmatrix} 1 & -\frac{K_o}{s} + (J_s + J_m)s + B_1 + B_2 \\ Y_a(s) & Y_a(s)\left[(J_s + J_m)s - \frac{K_o}{s} + B_1 + B_2\right] + 1 \end{bmatrix} \begin{bmatrix} T_d \\ \omega_{cs} \end{bmatrix} \tag{42}$$

Now that both the two-port model of the system and the desired transfer function are specified and ensured to be in proper form, the actuation impedance is synthesized. Due to the two-port model form, we have four equations with four unknowns to solve. The elements H_{11}, H_{12}, and H_{21} are equivalent to unspecified unknown frequency responses, and H_{22} is equivalent to the desired frequency response,

$$\begin{aligned} H_{11} &\Rightarrow \tilde{A} = U_{11} \\ H_{12} &\Rightarrow \tilde{B} = U_{12} \\ H_{21} &\Rightarrow \tilde{C} = U_{21} \\ H_{22} &\Rightarrow \tilde{D} = \frac{1}{(J_s+J_m)s - \frac{K_o}{s} + B_1 + B_2 + 1/Y_a} \cdot \left[\frac{\frac{1}{\alpha\tau_1}+1}{\frac{1}{\tau_1}+1} \cdot \frac{\frac{1}{\tau_2/\alpha}+1}{\frac{1}{\tau_2}+1} \right]^n \end{aligned} \tag{43}$$

Solving the system of equations (43) provides not only the resulting impedance function of the unknown impedance function $Z(s)$, but also the other relations in the two-port system (U_{11}, U_{12}, U_{21}). The resulting frequency response for the transfer functions of each element of the two-port matrix are summarized in Figure 34. As seen in the graphs, the frequency response

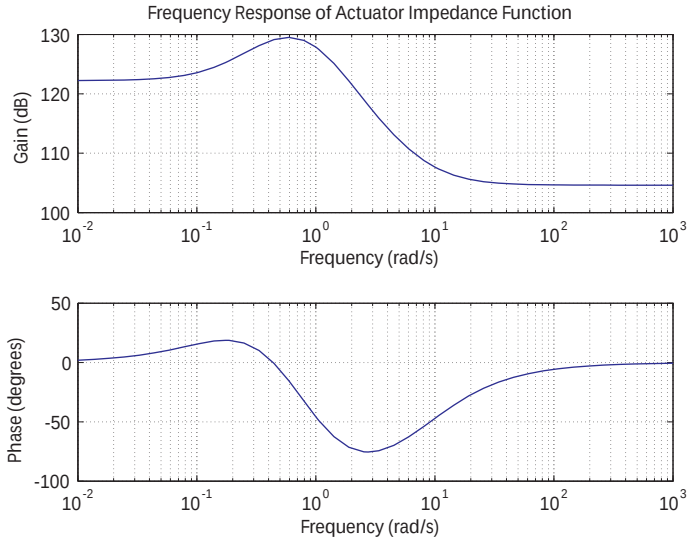

Figure 35: Frequency response of the synthesis derived actuation impedance function for the control surface system.

for H_{22} matches the specified response. Additionally, the resulting impedance function for $Z(s)$ is found as in equation (44). This impedance function relates the difference in velocity between the submarine base and the control surface to a torque required by an actuator system, so it is expressed as an *actuator* impedance,

$$Z_a(s) = \frac{a_4 s^4 + a_3 s^3 + a_2 s^2 + a_1 s + a_0}{b_4 s^4 + b_3 s^3 + b_2 s^2 + b_1 s + b_0} \tag{44}$$

where $a_4 = 2.63 \times 10^{18}$, $a_3 = 3.42 \times 10^{19}$, $a_2 = 9.50 \times 10^{19}$, $a_1 = 4.55 \times 10^{19}$, $a_0 = 5.00 \times 10^{18}$, $b_4 = 1.55 \times 10^{13}$, $b_3 = 4.43 \times 10^{13}$, $b_2 = 4.72 \times 10^{13}$, $b_1 = 2.22 \times 10^{13}$, and $b_0 = 3.87 \times 10^{12}$. The actuation impedance function has a frequency response as seen in Figure 35. The actuation frequency response peaks at 0.6 rad/s which means that the torques provided by the actuation function are the greatest at that point. A positive real test reveals that equation (44) is a positive real function, which implies a purely passive realization of the function is permissible. However, further investigation indicates that positive real pole removal is required at values other than $s = 0$ or $s = \infty$. As a result the fourth order synthesized impedance requires either complex coupled Brune elements or active components for realization [28, 79].

C.3 Impedance Expansion

Using partial fraction expansion, the actuation impedance function, $Z_a(s)$, can be expanded into separate terms so that individual impedance function components can be identified.

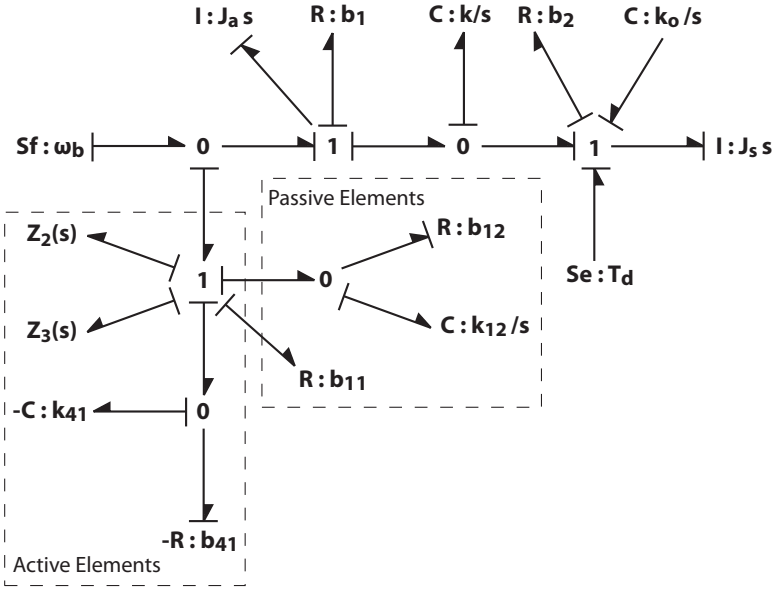

Figure 36: Synthesized bond graph elements separated into both active and passive components.

Partial fraction expansion of equation (44) yields,

$$\begin{gathered} Z_a(s) = Z_{active}(s) + Z_{passive}(s) \\ Z_{active}(s) = \frac{1}{\frac{s^2}{k_{22}}+\frac{s}{k_{21}}+\frac{1}{b_{21}}} + \frac{1}{\frac{s^2}{k_{32}}+\frac{s}{k_{31}}+\frac{1}{b_{31}}} + \frac{1}{\frac{s}{k_{41}}+\frac{1}{b_{41}}} \\ Z_{passive}(s) = b_{11} + \frac{1}{\frac{s}{k_{12}}+\frac{1}{b_{12}}} \end{gathered} \tag{45}$$

enabling us to partition the actuator impedance into separate active and a passive components, based on the required form of a positive real function. For the specific case examined here, for example, we can obtain passive parameters $b_{11} = 1.70 \times 10^5$ N/s, $k_{12} = 9.16 \times 10^7$ N-m/rad, and $b_{12} = 1.10 \times 10^8$ N/s, and active parameters $k_{21} = 4.82 \times 10^6$ N-m/rad, $b_{21} = 1.61 \times 10^7$ N/s, $k_{22} = 5.79 \times 10^6$ N-m/rad, $k_{31} = 1.04 \times 10^7$ N-m/rad, $b_{31} = 2.49 \times 10^7 N/s$, $k_{32} = 1.73 \times 10^7$ N-m/rad, $k_{41} = -8.98 \times 10^7$ N-m/rad, and $b_{41} = -1.50 \times 10^8$ N/s.

The active components are either negative impedances or non-realizable complex impedance elements which cannot be represented by simple impedance components. The passive actuation components have basic impedance relations that can be realized as physical elements such as rotational springs and dampers. The full bond graph representation of the derived impedance function within the framework of the control surface system is shown in Figure 36.

C.4 Purely Active Realization of Synthesized System

If the passive and active components of the synthesized impedance function are not separated, then the derived impedance function is ultimately represented by a single modulated-effort source, as shown in Figure 37. The modulation of the torque source is prescribed by the

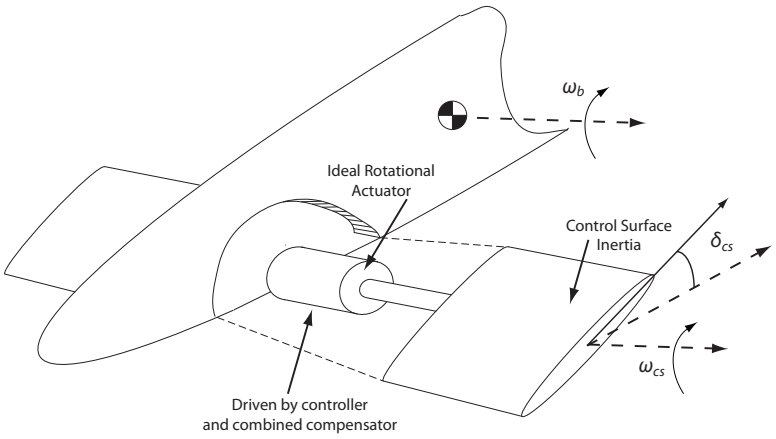

Figure 37: Control surface system realization with ideal rotational actuator.

derived actuation impedance function. For the torque source, the output effort (T_a) is related to the flow signal (ω_{11}) via the transfer function of the active elements. Using the state equations derived for the active elements in equation 46, a compensator controller function can be derived in state space form,

$$\begin{aligned}
\dot{\theta}_{12} &= \omega_{11} - \tfrac{k_{12}}{b_{12}}\theta_{12} \\
\dot{\theta}_{21} &= \omega_{11} - \tfrac{k_{21}}{b_{21}}\theta_{21} - \tfrac{k_{21}}{k_{22}}\theta_{21} \\
\dot{\theta}_{31} &= \omega_{11} - \tfrac{k_{31}}{b_{31}}\theta_{31} - \tfrac{k_{31}}{k_{32}}\theta_{31} \\
\dot{\theta}_{41} &= \omega_{11} - \tfrac{k_{41}}{b_{41}}\theta_{41}
\end{aligned} \tag{46}$$

where passive parameters are $b_{11} = 1.70 \times 10^5$ N/s, $k_{12} = 9.16 \times 10^7$ N-m/rad, and $b_{12} = 1.10 \times 10^8$ N/s, and active parameters $k_{21} = 4.82 \times 10^6$ N-m/rad, $b_{21} = 1.61 \times 10^7$ N/s, $k_{22} = 5.79 \times 10^6$ N-m/rad, $k_{31} = 1.04 \times 10^7$ N-m/rad, $b_{31} = 2.49 \times 10^7$ N/s, $k_{32} = 1.73 \times 10^7$ N-m/rad, $k_{41} = -8.98 \times 10^7$ N-m/rad, and $b_{41} = -1.50 \times 10^8$ N/s. Using the above differential equations, the specified torque output of the ideal actuator as related to the difference angular velocity, ω_{11} (difference between the submarine pitch rate and the control surface rate), results from the summation of the impedances given by,

$$T_a = b_{11}\omega_{11} + k_{12}\theta_{12} + k_{21}\theta_{21} + k_{31}\theta_{31} + k_{41}\theta_{41} \tag{47}$$

Representing equation (47) in block diagram form results in a controller algorithm that utilizes the parameters derived directly from the synthesis method. Figure 38 depicts the controller form integrated with the bond graph structure.

C.5 Separated Active and Passive Subsystem Realization

As in the active suspension example, separation of the passive elements reduces the control algorithm by eliminating passive elements from the function and physically realizing them as passive components. For the sake of comparison, the energy consumption should be compared between both the pure active case and the separated passive case.

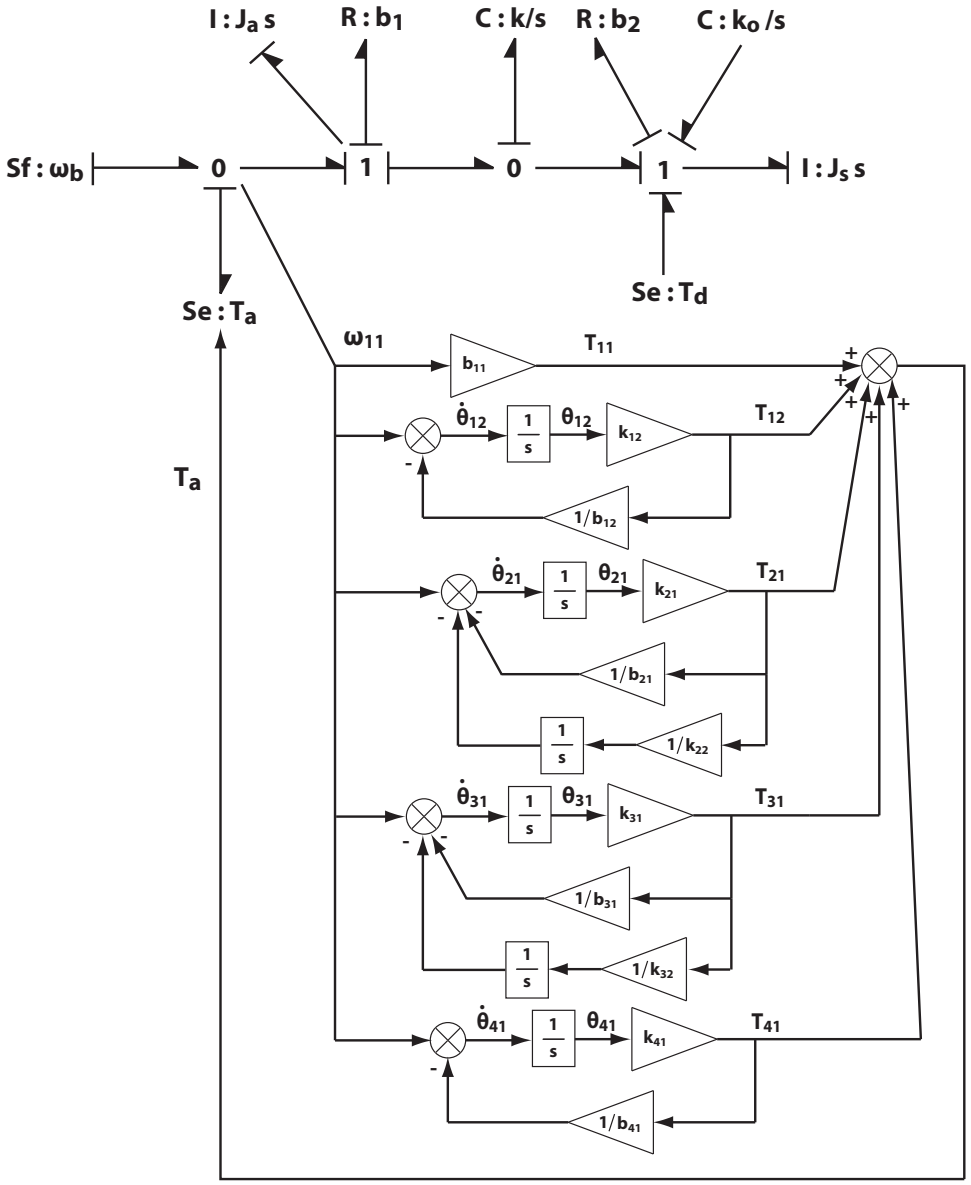

Figure 38: Torque source controller algorithm as determined by the synthesis expansion incorporated in the bond graph structure.

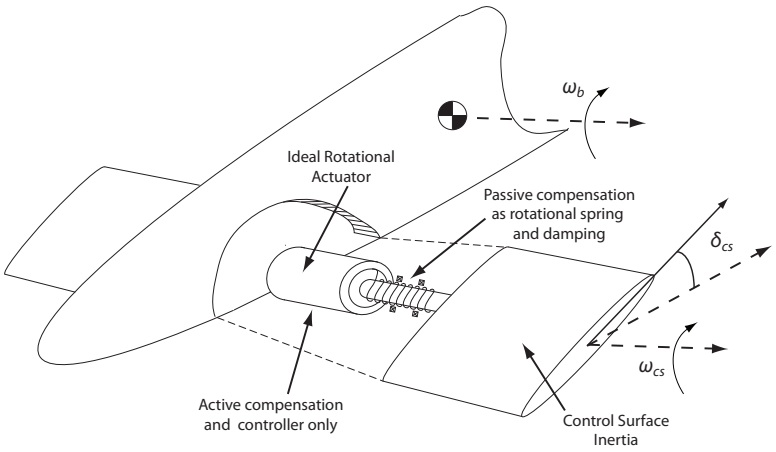

Figure 39: Control surface system realization with passive components separated.

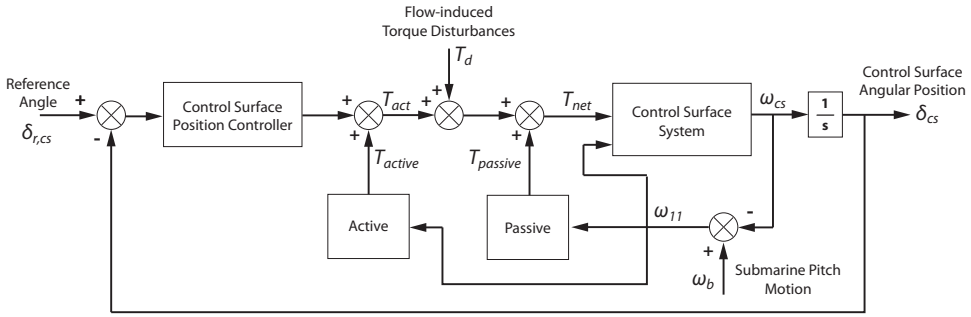

Figure 40: Block diagram representation of control surface system and compensator.

By separating the active and passive components, a modulated effort source and a passive spring damper system represent the derived impedance functions, as shown in schematically in Figure 39, or in block diagram form in Figure 40. The modulation of the torque source is governed by the derived actuation impedance function.

For the modified torque source, the transfer function of the active elements without the passive components relates the output effort (T_a) via the flow signal (ω_{11}). Using the state equations derived from the active elements in equation (48), the compensator controller function state equations are,

$$\begin{aligned} \dot{\theta}_{21} &= \omega_{11} - \frac{k_{21}}{b_{21}}\theta_{21} - \frac{k_{21}}{k_{22}}\theta_{21} \\ \dot{\theta}_{31} &= \omega_{11} - \frac{k_{31}}{b_{31}}\theta_{31} - \frac{k_{31}}{k_{32}}\theta_{31} \\ \dot{\theta}_{41} &= \omega_{11} - \frac{k_{41}}{b_{41}}\theta_{41} \end{aligned} \tag{48}$$

where the parameters remain identical to those given above for equation (46). Again, the specified torque output of the ideal actuator is related to the difference angular velocity, ω_{11}, and is the summation of the impedances,

$$T_a = b_{11}\omega_{11} + k_{21}\theta_{21} + k_{31}\theta_{31} + k_{41}\theta_{41} \tag{49}$$

Representing the modified controller function equation (49) in block diagram form results in a modified controller algorithm, this utilizes the parameters derived from the synthesis method. Figure 41 depicts the controller integrated within the bond graph structure.

C.6 Model Reduction of Synthesized Impedance

The fourth order complexity of the synthesized impedance function complicates the realization procedure. Although the complex impedance function yields positive real characteristics, a purely passive realization of the function could not be completely derived due to function complexity. A purely passive realization of the fourth order system with complex roots requires coupled passive elements as shown in Temes [79]. Coupled passive elements are physically difficult to realize in many physical domains and should be avoided while using synthesis techniques.

The order of a given system can always be reduced via balanced realization with increasing error depending on the magnitude of the state contributions. The interested reader can find additional coverage of the balanced realization procedure in Appendix D. The original actuator impedance function,

$$Z_a(s) = \frac{a_4 s^4 + a_3 s^3 + a_2 s^2 + a_1 s + a_0}{b_4 s^4 + b_3 s^3 + b_2 s^2 + b_1 s + b_0} \tag{50}$$

can be converted to the state space form,

$$Z_a(s) = \left[\begin{array}{cccc|c} -2.867 & -3.055 & -1.433 & -0.25 & 1 \\ 1 & 0 & 0 & 0 & 0 \\ 0 & 1 & 0 & 0 & 0 \\ 0 & 0 & 1 & 0 & 0 \\ \hline 1.725e6 & 5.628e6 & 2.698e6 & 2.873e5 & 1.702e5 \end{array}\right] \tag{51}$$

Computing the balanced realization of the impedance space state function produces both the balanced state space realization as well as the error G vector. The error G vector for $Z_a(s)$ is given by,

$$G_{error} = \left[\begin{array}{cccc} 1.5235 & 0.8543 & 0.0972 & 0.0026 \end{array}\right]^T$$

The order of magnitude drop between the second and third entries in the error G vector implies that an accurate realization of a second order system exists for $Z_a(s)$. The relative contributions from the balance third and fourth states are an order of magnitude less than the contributions of the first and second states. The reduced order $Z_a(s)$ system is procured by elimination of the low contribution states shown in equation (52).

$$Z_{red}(s) = \left[\begin{array}{cc|c} -0.7043 & -0.6297 & -1465 \\ 0.6297 & -0.0484 & 287.7 \\ \hline -1465 & -287.7 & 1.702e5 \end{array}\right] \tag{52}$$

Conversion of the second order state space representation to a SISO transfer function pro-

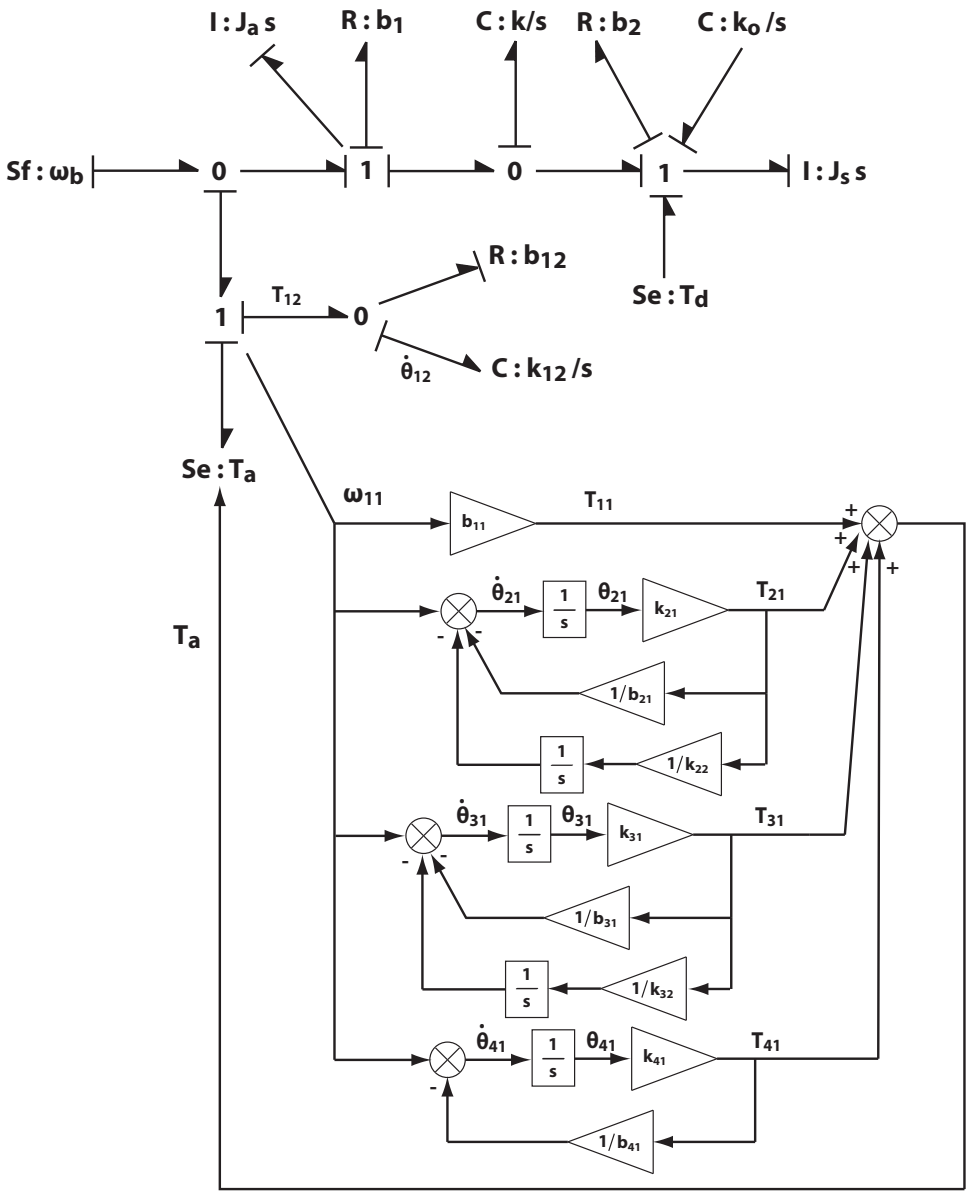

Figure 41: Torque source controller algorithm with passive components separated.

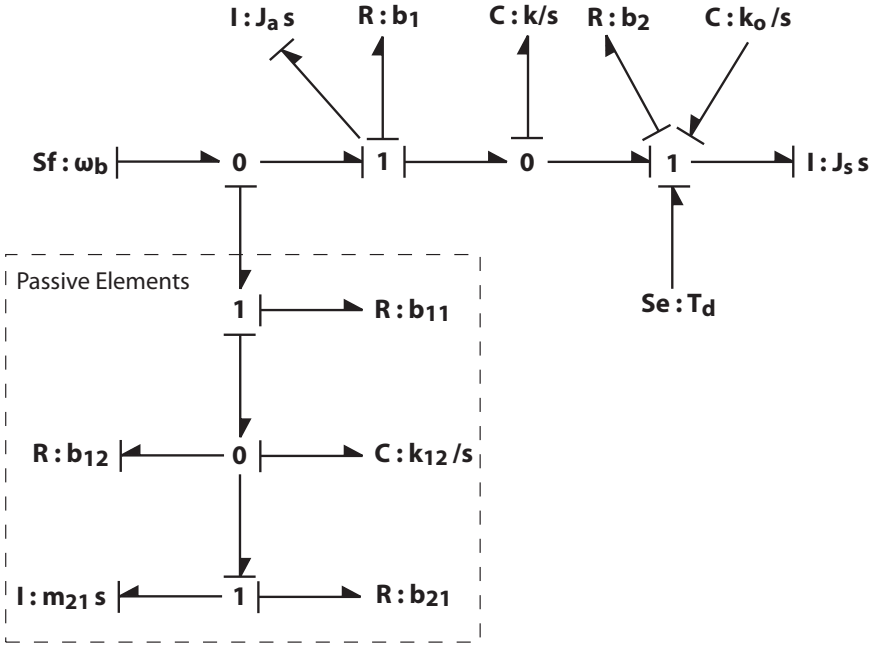

Figure 42: Reduced order impedance function in bond graph form yielding a purely passive system.

duces the reduced impedance function,

$$Z_{red}(s) = \frac{1.702 \times 10^5 s^2 + 2.192 \times 10^6 s + 6.498 \times 10^5}{s^2 + 0.7527 s + 0.4306} \tag{53}$$

The reduced actuation function has a frequency response as shown in Figure 18. For comparison, the frequency response plot also contains the original synthesized impedance function. Since the original impedance function is a positive real function, the reduced order system also is positive real such that a purely passive realization of the function must exist. Due to the order reduction, the realization of the impedance function with desired response yields a less complicated result which can more readily be physically constructed. Continuous fraction expansion of the $Z_{red}(s)$ function produces equation (54).

$$Z_{red}(s) = b_{11} + \cfrac{1}{\frac{s}{k_{12}} + \cfrac{1}{b_{12}} + \cfrac{1}{m_{21}s + b_{21}}} \tag{54}$$

where $b_{11} = 1.70 \times 10^5$, $k_{12} = 2.06 \times 10^6$, $b_{12} = 4.36 \times 10^6$, $m_{21} = 6.917 \times 10^6$, and $b_{21} = 1.932 \times 10^6$. Since all element coefficients from the resulting function expansion are positive real values, the total function is purely passive. The full bond graph representation of the reduced impedance function within the framework of the control surface system is shown in Figure 42.

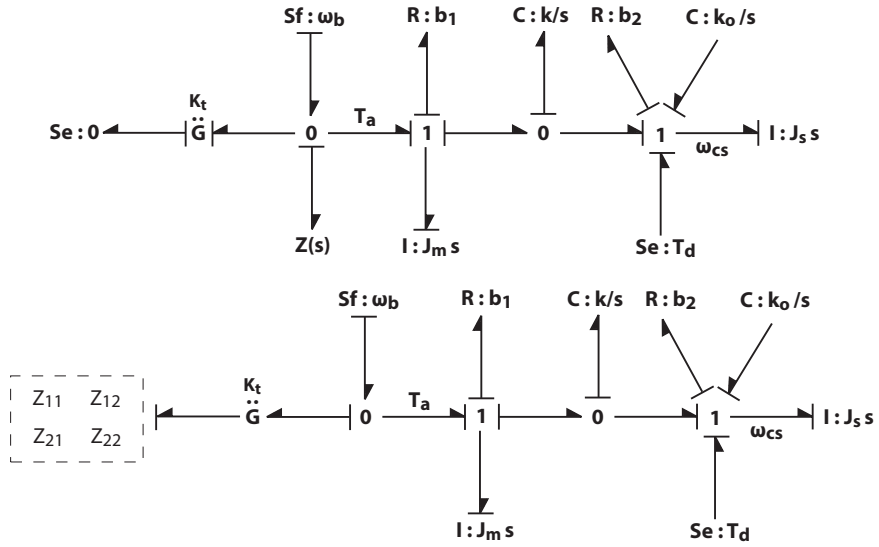

Figure 43: Original pure mechanical domain system and the new partially electrical domain system with unknown equivalent two-port impedance function.

C.7 Equivalent Impedance Transformation

To find the equivalent impedance of the new modified bond graph via secondary synthesis, the original bond graph transmission matrix must equate to the modified transmission matrix. Figure 43 shows the original bond graph with the flow source reverted to the original negative impedance function that was derived and the pure hydraulic form bond graph. Converting the compensator algorithm back into an impedance function ensures that any necessary modifications to the controller are accounted for.

For each bond graph, the two-port transmission matrices must be found for modified portions of the bond graph. Since no changes occur beyond the synthesized impedance function, the remaining portions of the bond graph are not needed for the two-port representation. Equation (55) illustrates the matrix function for the original case with a placeholder gyrator element added, and equation (56) displays the matrix function for the electrical conversion.

$$\begin{bmatrix} 0 & K_T \\ \frac{1}{K_T} & 0 \end{bmatrix} \begin{bmatrix} 1 & 0 \\ \frac{1}{Z_{red}(s)} & 1 \end{bmatrix} = \begin{bmatrix} \frac{K_T}{Z_{red}(s)} & K_T \\ \frac{1}{K_T} & 0 \end{bmatrix} \tag{55}$$

In the case for the electrical conversion, the equivalent two-port impedance is unknown and thusly represented as a matrix of unknowns.

$$\begin{bmatrix} Z_{11} & Z_{12} \\ Z_{21} & Z_{22} \end{bmatrix} \begin{bmatrix} 0 & K_T \\ \frac{1}{K_T} & 0 \end{bmatrix} = \begin{bmatrix} \frac{Z_{12}}{K_T} & K_T Z_{11} \\ \frac{Z_{22}}{K_T} & K_T Z_{21} \end{bmatrix} \tag{56}$$

For each two-port representation to have equivalent impedance matrices, the derived two-port matrices must be identically equal. Solving for the unknown Z matrix, the equivalent

structure is found in equation (57).

$$\begin{bmatrix} Z_{11} & Z_{12} \\ Z_{21} & Z_{22} \end{bmatrix} = \begin{bmatrix} 1 & \frac{K_T^2}{Z_{red}(s)} \\ 0 & 1 \end{bmatrix} \tag{57}$$

The impedance function derived in the above equation has the *structure* of a 1-junction where the impedance is composed of the inverse of the elements off the junction. However, due to the gyrator modulus, there is an additional scaling factor on all of the impedance elements. To compensate for the gyrator modulus, the coefficients of the impedance elements must be scaled accordingly. The resulting equivalent impedance function takes the form,

$$Z_{eq}(s) = \frac{1}{\frac{b_{11}}{K_T^2} + \frac{1}{m_{12}K_T^2 s + b_{12}K_T^2 + \frac{1}{s/k_{21}K_T^2 + s/b_{21}K_T^2}}} \tag{58}$$

where $b_{11} = 1.70 \times 10^5, m_{12} = 2.06 \times 10^6, b_{12} = 4.36 \times 10^6, k_{21} = 6.917 \times 10^6, b_{21} = 1.932 \times 10^6$ and K_t is any positive real number. With these modified parameters and the structure from the two-port secondary synthesis, the new bond graph structure can be generated.

Figure 44 shows the new bond graph layout of the electrical conversion realization of the control surface ocean disturbance rejection compensator. Realization of the gyrator and electrical domain portion of the bond graph yields Figure 21. The gyrator represents the ideal torque source actuation. Moving the compensation function from the mechanical domain to the electrical domain produces an internal voltage filter which indirectly filters the torque supplied to the control surface system.

D Balanced Realization

In the case of several of the derived impedance functions found throughout this report, the order of the resulting function was the magnitude of both the order of the model function and the desired response function. For example, a second order model with an unknown impedance function that is run through the synthesis procedure with a desired response of a second order system procures a fourth order impedance function. Higher order impedance functions tend to be physically difficult to realize and even more difficult to physically manufacture. Additionally, high order functions that are found to be positive real often cannot easily be decomposed into purely passive elements without significant function manipulation.

One potential method for impedance model simplification is order reduction of the function [58]. Reliable reduction of model order can be achieved by internally balancing the model system. This balanced realization contains the original number of states, but readjusts the state space values so that the relative contributions from each state are in descending order.

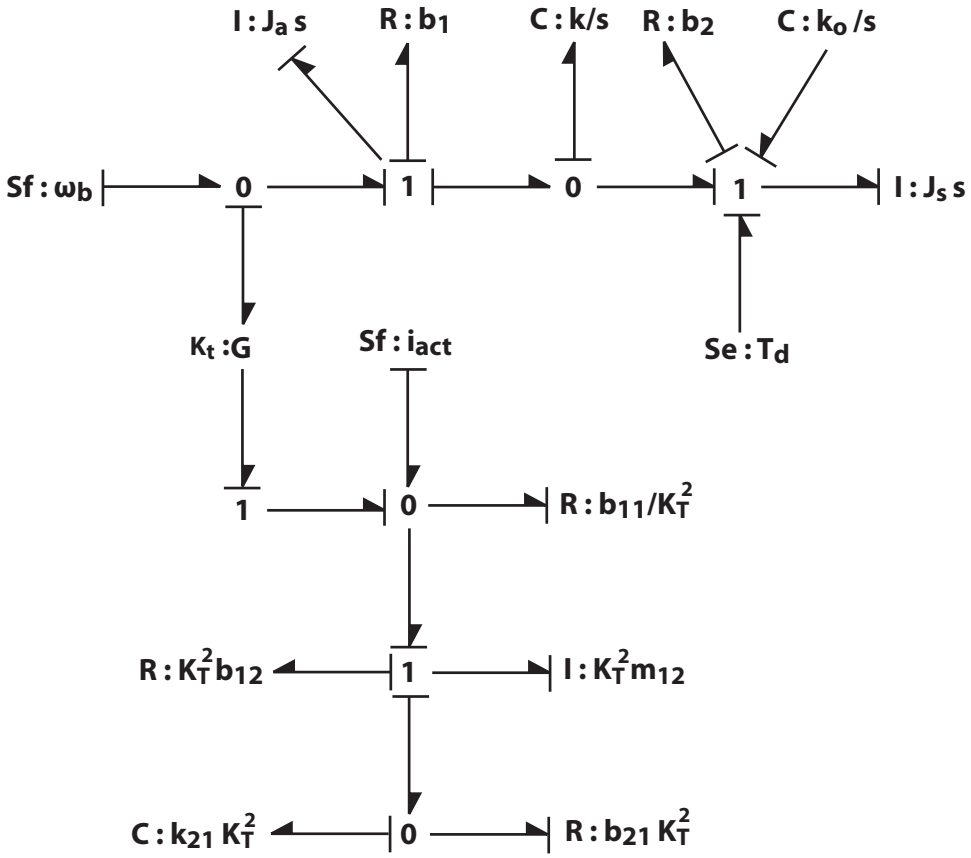

Figure 44: Passive compensation as realized in electrical form inside electromechanical actuator.

D.1 Conditions for a Balanced Realization

Consider a large order impedance transfer function $Z(s)$ which must be either proper or strictly proper. By the definition of the transfer function, the function $Z(s)$ can be converted from transfer function form to the state space form.

$$Z(s) = \frac{N(s)}{D(s)} \Rightarrow \begin{array}{l} \dot{x} = Ax + Bu \\ y = Cx + Du \end{array}$$

A state coordinate transformation ($\hat{x} = Tx$) can be performed on the state space representation of the function $Z(s)$. This similarity transformation results in an equivalent system as shown.

$$\begin{array}{l} \hat{\dot{x}} = TAT^{-1}\hat{x} + TBu \\ y = CT^{-1}\hat{x} + Du \end{array}$$

In the case of a balanced realization, the unique transformation T, when applied to both the observability gramians (L_o) and controllability gramians (L_c), results in modified gramians that are equivalent. The modified gramians are given as,

$$\begin{array}{l} \hat{L}_o = T^{-T} L_o T^{-1} \\ \hat{L}_c = T L_c T^T \end{array}$$

In the case of an internally balanced realization when the modified gramians are equivalent, the resulting structure of the modified gramians is in diagonalized form,

$$\hat{L}_o = \hat{L}_c = diag(g_1,\ g_2, \ldots,\ g_n)$$

where the diagonal terms are in descending order ($g_1 \geq g_2 \geq ? \geq g_n$). Reduction of system order eliminates states from the balanced realization system according to the diagonalized gramians form. A proper model reduction identifies an order of magnitude drop in the diagonalized matrix as an indication of decreasing state contributions. The states of the balanced realization at this division are eliminated, which reduces the model order. A reduction to any order is possible, however reduction errors become ever more present with increasing order reduction,

$$\left\| G(s) - G_{approx}(s) \right\|_\infty = 2 \sum_{k=m+1}^{n} \lambda_k$$

The errors of the model reduction are bounded by the sum of the eliminated states from the diagonalized matrix gramian forms.

D.2 Method to Determine Balanced Realization

To determine the unique transformation T that yields the balanced realization, an algorithmic process that produces a decomposition of one of the gramians is found to produce equivalent controllability and observability gramians [58]. The following procedure for procuring

the unique transformation is implementable in the MATLAB environment with the "balreal" command.

1. The observability gramian must be factored into two equivalent matrices with one being orthogonal to the other.
$$L_o = R^T R$$
where the matrix R cannot be singular.

2. Combining the R matrix found from the observability gramian with the controllability gramian produces an altered controllability matrix. Decomposing the new matrix into Eigenvalue and eigenvector matrices yields the following:
$$RL_cR^T = U\Lambda^2 U^T$$
where U are the eigenvectors which combine to form an orthogonal unitary matrix and Λ is a diagonal matrix comprised of the Eigenvalues.

3. The following procedure yields the unique transformation that produces the balanced realization. The matrix T is defined as follows:
$$T = R^{-1}U\Lambda^{1/2}$$

E Passivity Conditions

Conditions exist which sufficiently indicate that a given impedance function is realizable via strictly passive elements [28]. However, note that satisfying these conditions does not imply that the passive realization of the system is succinctly derived with straightforward techniques. Complex manipulations and couplings of impedance functions are sometimes required to generate a purely passive realization, especially in the case of high order impedance functions. The following definitions provide the outlines of the composition of passively realizable systems in terms of all bond graph elements.

E.1 One-Port Passive System Conditions

The location of the poles and/or zeros in a given polynomial function is an important concept when dealing with the complex s-domain. Many insights into the function response and type derived from the location of poles and zeros in the complex s-domain.

Definition 1 *A given polynomial function, A(s), in the s-domain is said to be a Hurwitz polynomial if*
$$A(s) = a_0 + a_1 s + \ldots + a_n s^n$$

1. *A(s) is a real polynomial, meaning that all values a_i are real coefficients.*
2. *All of the zeros of A(s) are in the left half-plane. Any zeros that lie on the imaginary axis must be simple zeros. (Re(s) ≤ 0).*

The polynomial A(s) is said to be a strictly Hurwitz polynomial if all the zeros are in the left half plane (LHP) without any zeros which lie on the j-axis. (Re(s) < 0).

Definition 2 *A one-port impedance function, Z(s), is said to be passively realizable if the given impedance function is found to be a positive real function [28].*

1. *The impedance function, Z(s), must be a real rational function of s.*

$$Z(s) = \frac{a_0 + a_1 s + \ldots + a_n s^n}{b_0 + b_1 s + \ldots + b_m s^m}$$

   where the coefficients a_i and b_i are all real values.

2. *For all real values of ω, the following condition is satisfied:*

$$\mathrm{Re} Z(j\omega) \geq 0$$

3. *All the poles of Z(s) are in the closed LHP of the s-plane.*

The third condition of positive realness on the pole locations can also be expressed in terms of Hurwitz polynomials. Depending on the polynomial type, the third condition is satisfied if the following conditions are met:

1. *The denominator of Z(s) must be either a Hurwitz or strictly Hurwitz polynomial.*
2. *If the denominator polynomial is only Hurwitz, then the zeros on the $j\omega$-axis must be simple. Additionally, the poles as $s \to \infty$ must also be simple.*

E.2 Methods for Determination of Positive-Realness

Simple tests have been found which provide insight into the positive real nature of a given function [79]. The first condition of positive realness is easily determined via inspection and verification of each polynomial coefficient being real valued. The second and third conditions are more difficult to ascertain and cannot be immediately found via inspection.

A technique which is a sufficient condition for proving $Re(j\omega) \geq 0$ (condition 2 for positive real functions given above), is Strum's theorem. Strum's theorem provides a method through

which the number of sign changes, meaning a simple real zero value, occur on the positive axis. Strum's theorem presents the following condition:

$$P(x) = a_n x^n + a_{n-1} x^{n-1} + \ldots + a_1 x + a_0 \geq 0$$

where $x \geq 0$ and the function $P(x)$ is found by division of the function of interest into even and odd polynomial values for both the numerator and denominator. The terms are then combined together as follows to produce P(x) where $\omega^2 = x$:

$$P(\omega^2) = N_{even}(j\omega) D_{even}(j\omega) - N_{odd}(j\omega) D_{odd}(j\omega)$$

The condition of Strum's theorem requires that $P(x)$ contain no simple real zeros on the positive interval, which satisfies $Re(j\omega) \geq 0$.

Sufficient conditions for the satisfaction of the third condition of positive realness can also be found via the manipulation of numerator and denominator of the function of interest. The following modification of the function $Z(s)$ must have all zeros in the open LHP:

$$Z_{\,\mathrm{mod}}\,(s) = \frac{N(s)}{D(s)} + 1 = \frac{N(s) + D(s)}{D(s)}$$

The modified function above implies that N(s) + D(s) must be strictly Hurwitz in order to have all zeros in the open LHP. Therefore, the addition of the numerator and denominator provides a quick test of the third condition of positive realness of a given function.

E.3 Extension to Two-port Systems

The prior discussion dealt only with the possibility of passive realization for a given one-port impedance transfer function. The following definition extends the previous definitions to encapsulate two-port functions [79]. As in the case of the one-port system, a two-port system must be a positive real function for a purely passive realization to exist.

Definition 3 *A two-port impedance function system given by a two-port matrix Z(s) is positive real if the following conditions are satisfied:*

1. *Z(s) exists and is analytic on the interval of $\sigma > 0$, where σ is the real portion of s ($s = \sigma + j\omega$).*
2. *$Z^*(s) = Z(s^*)$ on the interval $\sigma > 0$, where the superscript asterisk indicates the complex conjugate.*
3. *$Z_H(s) \geq 0$ on the interval $\sigma > 0$, where $Z_H(s)$ designates the Hermitian portion of the matrix.*

The above conditions for positive realness of two-port systems can also be expressed in a

perhaps more readily understood form. The following conditions are equivalent to the initial three of the definition:

1. *All elements of Z(s) are real rational functions.*
2. *Z(s) contains no poles in the range of* $\sigma > 0$.
3. *The poles of Z(s) on the* $j\omega$*-axis are simple values.*
4. *For the poles on the* $j\omega$*-axis, the residues of each element must be simple values.*
5. $Z_H(j\omega) \geq 0$ *for all real values of* ω.

List of Figures

List of Tables